*J. Indian Inst. Sci.*, Nov.–Dec. 2005, **85**, 319–352


# Molecular dynamics simulations of matrix trapped molecules

Y. HAAS AND D. SCHWEKE
Department of Physical Chemistry and the Farkas Center for Light Induced Processes,
The Hebrew University of Jerusalem, Jerusalem, Israel.
email: yehuda@chem.ch.huji.ac.il.

Received on May 19, 2005.

**Abstract**

The use of molecular dynamics (MD) to simulate the structure of trapping sites of molecules in cryogenic matrixes is surveyed, with an emphasis on work from the authors' laboratory. After commenting on the methods used to simulate the trapping of small symmetric molecules, recent attempts to use the method for medium sized molecules and clusters (about 20–30 atoms) are described. In particular, the study of low-symmetry molecules such as propyl–benzene, phenylpyrrole and pyrrolobenzonitrile are described. The structures of the sites help in understanding the spectra and photochemistry of these molecules in cryogenic matrixes. A complete simulation of the IR or UV spectra of trapped molecules requires a methodology for calculating the energy levels in a matrix, based on the structures obtained by MD. The current state of the art is briefly reviewed and possible pending advances are discussed.

**Keywords:** Matrix isolation, trapping site, molecular dynamics, spectroscopy, charge transfer, phenylpyrrole, pyrrolobenzonitrile.

## 1. Introduction

Matrix isolation was initially used for trapping and characterizing reactive species. Over the years the scope of this technique was broadened and it now also deals with the spectroscopic properties and reactivity of many stable molecules. While various matrix materials have been used extensively, this paper will discuss trapping in rare gas matrixes only.

Rare gas matrixes are among the ‘simplest’ environments in which a gas-phase molecule can be located (in the sense that their interaction with the molecule is small compared to intramolecular interactions) and experimentally easy to realize. This medium has therefore been attractive as a test ground for simulating the effect of the environment on the spectroscopic and chemical properties of trapped molecules. The small electron–phonon coupling characteristic for these materials results in weak phonon sidebands and thus narrow and well-resolved spectra. Several reviews on matrix-isolation research amply cover the literature prior to 1998 [1–4]. The goal of this paper is to survey recent work in the field with an emphasis on the application of MD simulations to clarify the effect of the structure on spectroscopic and dynamic properties. We shall therefore dwell mainly on advances after 1998 and highlight the efforts to elucidate the structure of trapping sites and their implications concerning the spectroscopic and chemical properties of molecules embedded in them. This

*Author for correspondence.

account is not meant to be exhaustive or comprehensive; rather it selectively summarizes the work in the authors' laboratory, including novel results, and also highlights some advances relevant to the main focus of the paper – the elucidation of environmental effects by realistic modeling. In recent years, advances in computer technology and in QC software made quantum mechanical calculations available to the whole chemistry community (rather than only to specialists). Even large molecules (10–20 heavy atoms) can now be treated fairly accurately, and experimental reports of spectra are usually accompanied by comparison to QC calculations. Most of the calculations still relate to the isolated molecules, rather to those interacting with the matrix. At the present rate of theoretical advances, the inclusion of such interactions will become possible in only a few years.

The paper is organized as follows: Section 2 introduces briefly the basic concepts of matrix isolation, trapping sites and the standard notation. Section 3 summarizes methods used to simulate site structure, with an emphasis on the method developed in Jerusalem and its ramifications. Section 4 (the main body of the paper) examines several typical systems trapped in matrix, starting from atoms, continuing with small molecules (that replace only one or two matrix atoms) and planar ones. For these systems an educated guess as to the shape and size of the trapping sites may be made intuitively. The last subsection deals with nonsymmetric molecules for which such a guess is much more speculative. In this section new results are reported. Section 5 surveys the methods used to simulate matrix shifts and Section 6 presents a summary and prospects for the future.

## 2. Principles of matrix isolation

A cryogenic matrix is usually prepared by spraying an inert gas on a window held at a temperature much lower than the melting point of the gas. The rate of cooling is too large for a single crystal to grow, rather a polycrystalline solid constructed of a large number of closely packed small crystallites is formed. Under these conditions amorphous solids are extremely difficult to grow and in most practical applications are not formed. As argon is the principal matrix host in the field, we shall use it as the standard material in this paper. Other rare gas atoms can be treated in an analogous fashion.

Pure argon crystallizes at low temperatures mainly in an fcc structure in the practical range of up to 40 K and atmospheric pressure. The (linear) dimension of the individual small crystallites ('grains'), estimated from line widths in X-ray and neutron diffraction, is under normal deposition conditions of the order of a few hundred Angstroms [5]. The grain is thus much larger than typical molecular dimensions and for practical applications may be treated as an infinitely large crystal. Trapping in grain boundaries is in principle possible; the guest is found in a less-ordered environment than when trapped in the bulk, and therefore inhomogeneous line broadening is expected. However, experience shows that sharp lines are normally found in the IR spectrum, so that trapping in grain boundaries appears to be a rare event which may be ignored. Annealing does not change the grain size, or the crystalline nature of the system. Thus, no major changes of the overall matrix structure take place in the small temperature range (30–35 K) used for annealing (in the case of argon heating above 39 K leads quickly to matrix loss due to the high vapor pressure). Annealing does affect small local defects and distortions due to small amplitude motions of argon at-

oms frozen during the deposition process in metastable sites. Therefore annealing does often allow distinction between sites of different stabilities.

Mixing of guests into argon solid ('seeding') could in principle result in a new thermodynamic stable phase, but this is rarely the case. Thus, small concentrations of guest molecules do not generally affect the X-ray diffraction of the samples, particularly the line widths, which are determined by the grain size [5]. The consensus is therefore that a matrix containing a guest is not a thermodynamic stable system; rather, the guest is forced into the host's matrix as an impurity and a seeded matrix may be considered as an organized crystal which is distorted only locally by the insertion of a guest.

It was found that when large amounts of guest molecules are mixed in, the argon matrix may assume an hcp structure [6], especially at high temperatures. When a large number of sites are observed spectroscopically, some workers assume that a 'local' hcp environment is created, which is equivalent to the formation of a stacking fault in the fcc lattice. (Recall that the fcc and hcp lattices differ only in the third crystal plane [7]). We shall assume in the following that the matrixes are dilute, and thus consider only the more stable fcc crystal structure in simulation attempts.

The upshot of this analysis is that in dilute matrixes the guest is considered to be in a 'cage' formed by its immediate neighboring host atoms, retaining elsewhere the overall fcc structure. Some minor distortions are possible as interaction with a guest molecule may shift argon atoms from their perfect crystal lattice position. In principle, two main types of cages that preserve long-range order in the matrix can be envisioned: a substitutional cage, in which one or more argon atoms are removed from the lattice and the guest inserted in their place, and an interstitial one, in which the guest is located in the free volume between neighboring atoms. As discussed in Sections 4.1 and 4.2, hydrogen and some other small atoms can be found in interstitial sites, but the stable location for larger atoms and molecules is ordinarily a substitutional site. Site-structure simulations aim at portraying the actual positions of all atoms in the matrix in the presence of the guest.

The properties of a cage are determined mainly by its size and shape. A molecule embedded in the cage may in principle assume several different orientations with respect to the neighboring matrix atoms. Each of the possible resulting structures is a trapping site. One orientation is frequently favored energetically over the others and therefore the distinction between a cage and a trapping site is often unimportant. In general, trapping sites for polyatomic molecules differ by the cavity size (the number of argon atoms removed from the lattice) and by the displacement of the remaining atoms from their perfect lattice position.

The difference between trapping sites is often revealed spectroscopically by the appearance of multiple bands due to a single molecular transition (in the IR, Raman or electronic spectra). Other causes for apparent band splitting such as formation of dimers or other aggregates may easily be distinguished experimentally. Spectroscopic site shifts are usually much smaller than the separation between neighboring molecular bands (e. g. vibrational ones) and can be experimentally observed if they are larger than the line widths. The width of molecular vibrational (or vibronic) bands is often determined by interaction with phonons; obviously, site splitting smaller than the width of the guest's bands, which cannot be experimentally observed, may be quite common.

Two main experimental techniques are used in the matrix field: optical spectroscopy and ESR. In this paper, we shall focus on the first method, which is subdivided into three main branches: IR, electronic (UV-VIS) and Raman spectroscopies. Most data are in practice obtained by the IR and UV-VIS techniques.

## 3. Computer simulations of matrix deposition using MD

Interpretation of matrix-based experiments requires a model for the intimate environment in which the guest finds itself. Earlier work on the topic was summarized in a review [1]; in 1994, Fraenkel and Haas [8] proposed a molecular dynamics method that attempts to mimic the 'real' matrix deposition process. A brief description of the method (simulation deposition method, SDM) is given in the Appendix. More recently, MD methods were used successfully by several authors to account for various experimental observations in cryogenic matrixes. In this section, a survey of recent advances in the MD simulation method is presented in order to highlight the various approximations used in the field and their consequences.

Ning and Qin [9] extended the SDM method and reported considerable reduction of computer time in the simulation by adopting a time-going-backwards technique. After constructing an initial guess matrix, the system is allowed to relax at 10 K and then is warmed up by backward integration to 130 K. At that temperature, the system is again allowed to relax, essentially 'erasing' any memory of the initial guess. Cooling back to 10 K by the usual method using the velocity reset method [10], the system is allowed to equilibrate and the geometry of the site is registered. A new run is started from this structure, repeating the process as many times as desired.

Crépin *et al*. [11] introduced some modifications in order to make the simulation more realistic. Periodic boundary conditions are used by many workers in order to eliminate artifacts due to 'edge' effects. In the case of argon matrixes, this practically forces one to use the {001} crystallographic plane as the plane on to which the guest molecule and the other argon atoms are added. However, it is well known that the crystal growth is mainly on the {111} plane, for which the use of periodic boundary conditions is more cumbersome as the boundaries are not mutually perpendicular. The use of the {001} plane for the template may bias the system in a nonrealistic way. In the F–H method, this difficulty is partly compensated for by randomly depositing argon atoms on the {001} plane prior to the guest molecule. Crépin *et al* discard the periodic boundary conditions and use instead a much larger template ($40 \times 40$ Å) and a cutoff distance of 15 Å. Another parameter used in the simulation is the time interval between the depositions of two argon atoms, which in a realistic experiment is about 40 ms, allowing complete thermal equilibration while in the MD simulation such a long delay is unrealistic. In most computer simulations the rate of deposition is much faster (10–20 ps intervals), Crépin *et al.* used 200 ps interval as a compromise.

Molnar, Horinek and Dick [12, 13] proposed a different simulation method in which a random search in the configuration space is performed for all possible trapping sites. In this random search model (RSM), the simulation starts by forming a cubic or spherical cavity in the center of a large cubic template of an argon crystal. Typically, 512 unit cells are used. Atoms are removed from the center of this template to form a 20 Å cavity into which the

guest molecule is inserted. The cavity must be much larger than the guest molecule to allow free translational and rotational motion of the latter. At this stage all argon atoms are rigidly held in their perfect lattice positions, and only the guest molecule is allowed to move. Next, argon atoms are forced into the cavity one by one to an unoccupied lattice position and the energy of the system is recalculated. The atom is rejected if the energy exceeds a predetermined threshold value. The insertions are performed at a rate slow enough to allow the guest molecule to accommodate itself in the smaller cavity. Towards the end of the simulation, the rejection rate increases considerably, and the threshold energy is increased gradually up to 10 times its initial value. At this point the cavity is practically full, as checked by the number of consecutive rejections of new argon atoms. The resulting structure (the 'static' trapping site is the first approximation to the site's geometry. In the second stage of RSM, three-dimensional periodic boundary conditions are imposed on the system. The structure is allowed to relax to a local minimum by letting all atoms except the boundary ones (the outermost layer) to move at a temperature of 10 K. A final check for the stability of the site is made by extracting the inner cluster of argon atoms surrounding the guest. The components of the cluster are allowed to interact for a time long enough to exchange energy, without periodic boundary conditions, allowing dissociation. A site is considered as unstable if one of the following conditions holds for its inner cluster:

(1) Argon atoms have evaporated from it.

(2) The temperature of the cluster exceeded a certain limit (typically 15 ps).

(3) The Verlet order parameter [14] dropped to 1/3 in the first 2–3 ps.

The method is in a way a brute force one, in which the density of argon atoms is increased until the 'internal pressure' generated exceeds a certain predetermined value.

A comparison between the RSM and the F-H methods was carried out for the deposition of anthracene [15] in an argon lattice. It was found that although the two methods use rather different stability criteria, the sites' distributions were rather similar.

## 4. Selected examples of some experimental studies and their simulation

In this section, we survey some recent experimental data on species trapped in cryogenic matrixes. The aim is to show how the spectroscopic observation of the splitting of molecular bands of a given transition may be explained by the existence of diverse trapping sites. The ultimate objective of the section is the description of the trapping of large asymmetric molecules, for which an initial guess for the structure of the cage is difficult to make. The simpler cases of smaller, symmetric guests are discussed first, beginning with a small guest (a hydrogen atom) who can accommodate itself in an interstitial site or an SS one. Analysis of the trapping of small molecules such as $CO_2$ and HONO that require the removal of only one or two argon atoms yet clearly occupy different sites is dealt with next. These small systems can usually be handled satisfactorily by simple initial guesses. The MD method was found to be particularly helpful with the interpretation of the electronic and vibrational spectra of relatively large planar molecules such as naphthalene, anthracene and porphyrin, which are the next topic. Asymmetric molecules are compared with these simpler systems in the last part of this section.

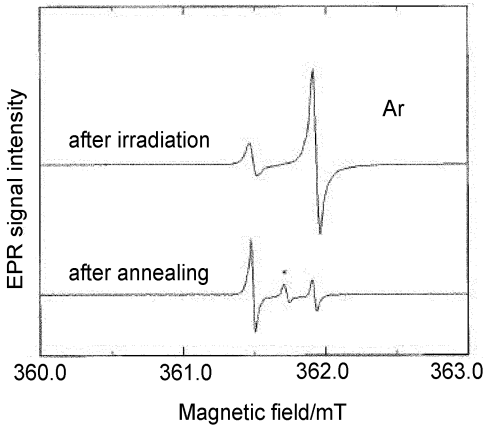


FIG. 1. A plot of the high-field portion of the EPR spectrum of hydrogen atoms isolated in an argon matrix at 14 K. The band marked by an asterisk is metastable and disappears upon warming to 16 K. The low and high field peaks are assigned to substitutional and interstitial sites, respectively (from ref. 16).

### 4.1. *Atoms*

Out of the extensive work on the trapping of atoms in rare gas matrixes, hydrogen atoms deserve special attention, being the smallest atoms and having been observed in many photochemical processes. In the context of this paper, the question is whether the trapping of even these small species can be successfully modeled. H atoms can be easily monitored by ESR spectroscopy, as shown in the example of an argon matrix in Fig. 1 [16]. The spectrum was obtained by depositing HBr in an argon matrix and irradiating at 193 nm. Different sites were distinguished by their different g-values and hyperfine constants, and by the different conduct under annealing. Peaks, whose intensity decreased upon annealing were assigned to interstitial sites and those whose intensity increased to substitutional ones. Similar results were obtained when HCl was used, and also with a krypton matrix.

The assignment was also supported by kinetic studies: interstitial H atoms are mobile, and their signal disappeared on warming, apparently due to recombination to a diamagnetic species. The atoms trapped in a substitutional site were found to be immobile. A molecular dynamics study was made to explain the trapping of H atoms in neon, argon, krypton and xenon matrixes [17]. A single hydrogen atom was introduced as a substitutional or interstitial impurity in a perfect fcc lattice consisting of 1371 or 1372 RG atoms, respectively. Initial conditions were generated by assigning to each atom a velocity randomly picked from the Maxwell–Boltzmann distribution at the desired temperature. Prior to collecting the atomic trajectories, the system was allowed to thermalize for 2.5 ps, during which period standard velocity scaling was applied to regulate the temperature. The system was then followed for an additional 37.5 ps as a micro-canonical ensemble, employing periodic boundary conditions.

It was found that in a neon matrix the H atom finds itself exclusively in a substitutional site. In argon or krypton matrixes both substitutional and octahedral (Oh) interstitial sites are stable. In the latter case, thermalization of the system results in considerable expansion of the cavity due to repulsive Ar–H interaction and subsequent lattice relaxation. In fact, the Oh site in argon is the smallest cavity where H atoms could be stabilized. Tetrahedral ($T_d$) sites were also considered, but MD trajectories initiated in these sites terminated in struc-

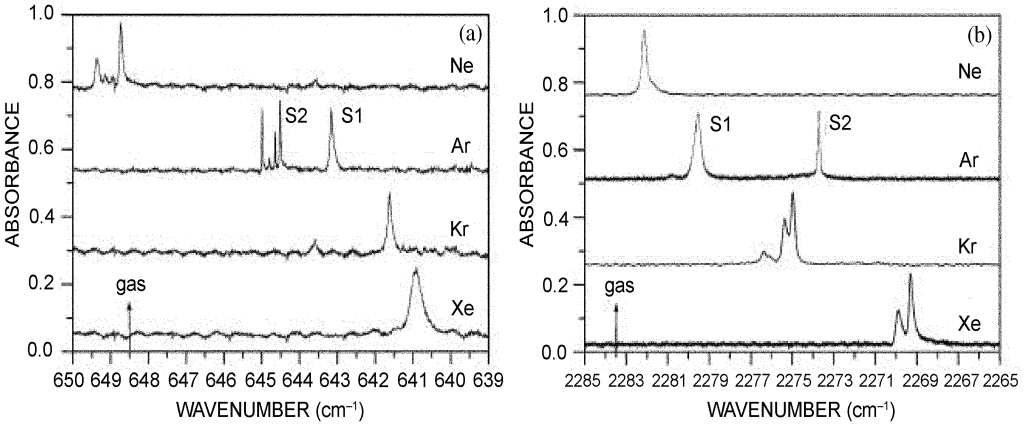


FIG. 2. Absorption spectra of $^{13}CO_2$ in rare gas matrixes at 5 K: (a) $n_2$ region, and (b) $n_3$ region (adapted from ref. 23).

tures with six nearest neighbors and internuclear distances similar to the Oh site. For xenon matrixes the model would suggest similar stability for both interstitial Oh and substitutional sites, whereas only one site is observed in the experiment! Based on the calculations the observed site can be assigned as a nearly undistorted substitutional site. This discrepancy raises the question whether all H atoms trapped in xenon are detectable by ESR spectroscopy. A more fundamental issue is whether the small size and mass of the hydrogen atom may require quantum mechanical treatment for a complete description of trapping.

### 4.2. *Small molecules*

For all larger systems, the consensus is that classical mechanics should be adequate for the description of the trapping in cryogenic matrixes (except perhaps in solid hydrogen, which is outside the scope of this paper).

#### 4.2.1. *$CO_2$*

This linear molecule was studied by several groups in different rare gas solids, mainly by infrared spectroscopy [18–23]. A recent experimental work compared the IR spectrum of $^{13}CO_2$ in neon, argon, krypton and xenon matrixes. Figure 2 shows the IR spectra obtained, from which it was concluded that only one trapping site (a di-substitutional (DS) one) is found in neon, two singly substituted ones (1SS and 2SS) in argon and only one 1SS site in krypton and xenon. These assignments agree with the previous work, and also with the expected trend based on the size of the rare gas atom. The observed small splitting of the $n_3$ mode in krypton and xenon was assigned to different orientations of the trapped molecule in an 1SS site, although no detailed calculations were presented. An extensive calculation of the site structure was made for $CO_2$ in argon, in which the trapping site structures were calculated by assuming pairwise potentials and calculating the site structure that best fits the experimentally observed shifts (see Section 5). Similar calculations were made on ozone [24] and $N_2O$ [25].

### 4.2.2. *HONO*

This molecule was extensively studied in matrixes due to its interesting infrared-induced photochemistry [26]. The molecule exists in two conformers that can be stabilized in a matrix, *syn* and *anti* (Fig. 3).

Mode-selective isomerization rates have been reported in a matrix [27], and many simulations were published, showing that the matrix actually enhances the reaction rate in comparison with the gas phase [28]. In krypton matrixes each vibrational band is split into two or three components, assigned to different trapping sites. Khriachtchev *et al*. [29] used a narrow-band tunable laser, to selectively excite the OH stretch vibration, leading to isomerization. Site selectivity was demonstrated in the sense that only molecules in the specific site pumped by the laser reacted; thus, energy transfer to neighboring trapped molecules did not occur. The nature of the trapping sites was guessed based on matrix shift of the vibrational bands. The red-shifted bands were attributed to 2SS site, while the blue-shifted ones were assigned to a more compact 1SS site.

Talik *et al.* [30, 31] studied the IR spectrum of the two isomers in an argon matrix using a different preparation scheme for HONO. It was also found that most bands of both isomers were split into two sub-bands while in the OH stretch region three sub-bands were found. The relative intensities and widths of the different sub-bands of a given vibrational transition were temperature dependent in a reversible way. In the case of the *anti*-isomer the widths of the two bands showed different temperature dependence, while in the case of the *syn* one, the widths of both the components varied in a similar fashion. Molecular dynamics simulations were performed in an attempt to confirm the hypothesis that the splitting was due to different trapping sites. For the more extended *anti*-isomer two trapping sites were found–a single substitutional one (A-SS) and a di-substitutional one (A-DS) which was found to be less frequently formed (in the ratio of 6:1). MD simulations were run with the {001} crystallographic plane facing the incoming molecules using a method similar to the Fraenkel–Haas one. In both the matrix sites the guest molecule was found to lie on the {001} plane with the center of mass of the molecule located almost exactly at the coordinates of a missing argon atom. For the SS site, 6 equivalent orientations are possible, while for the DS one, in which the molecule practically occupies only one lattice position with the OH end pointing towards the second missing argon atom, only two equivalent locations are possible (one for each missing argon atom). It was found that the molecule could rotate in both the trapping sites but more easily in the A-SS site than in the ‘larger’ A-DS one! This counterintuitive result was tentatively explained by the larger anisotropy of the DS site, in which the preferred orientations are relatively more stable with respect to rotation than in the SS site. However, energy calculations were not reported. On the basis of this calculation, the observed bands showing more pronounced temperature dependence were assigned to the A-SS site.

In the case of the more compact *syn*-isomer, only a single one-atom trapping site (S-SS) was found in the MD simulation. The appearance of two bands in the IR spectrum was not explained simply by the co-existence of the two trapping sites. The authors considered several options: different orientations in an SS site, existence of two different forms of argon (fcc and hcp) and modulation of the vibrational frequencies by the argon lattice phonons.

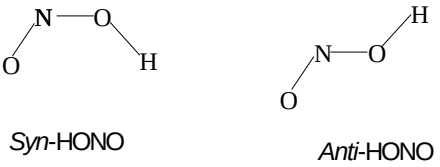


FIG. 3. The *syn–anti* isomerization of HONO.

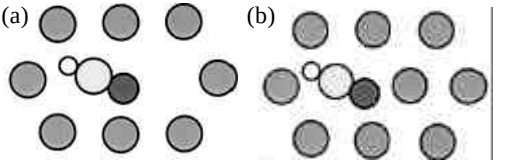


FIG. 4. The two trapping sites of HKrF in a krypton matrix; (a) is a double substitutional site, and (b) a single substitutional one (from ref. 33).

These ad-hoc rationalizations are questionable, as they should apply to the *anti*-isomer as well as to the *syn* one. The lack of energy calculations makes it difficult to assess the importance of each option properly.

It may be added, that in view of other simulations, another option may be considered, namely, an SS site in which the molecule is oriented along the {111} plane. The simulation method may have a bias for the {001} plane, as noticed by other workers. The separation between two adjacent layers in the {111} plane is larger than the distance between the two adjacent {001} layers. The effect of the trapped molecule on other layers was not explicitly discussed in the paper. It might be interesting to check whether an SS site with a {111} orientation might not be the second trapping site for both the isomers.

### 4.2.3. *HArF and HKrF*

These novel molecules were synthesized by Petersson, Lundell, Räsänen and coworkers [32, 33] by photo-dissociation of HF in an argon or krypton matrix, followed by gentle annealing. The molecules, characterized by their infrared spectra and kinetic behavior, were found to occupy different matrix sites distinguished by different spectral shifts and thermal annealing. For instance, the spectrum of HKrF revealed three pairs of absorption peaks: at 1951.6 and 1925.4 $cm^{-1}$, 650.9 and 645.9 $cm^{-1}$ and 417.0 and 414.2 $cm^{-1}$ [33]. By isotopic substitution and comparison with quantum chemical calculations, they were assigned to the H-Kr stretch, bend and Kr-F stretch, respectively. The assignment to two trapping sites is supported by the fact that upon annealing, the intensity of one set increased at the expense of the other, and thus was considered to be due to the more stable trapping site. The trapping sites were simulated by a simple model assuming that they were either SS or DS (Fig. 4). The energy of the SS one was calculated to be lower than that of the DS, but for HArF the energy order is reversed [34]. The DS site can convert to the more compact SS one by migration of a krypton atom to fill the vacancy near the HRgF molecule (Rg–rare gas).

As the figure indicates, the molecule occupies a {111} crystallographic plane. The analysis of the formation of these interesting compounds shows that the initial photodissociation of HF shoots the hydrogen away from the heavier F atom. The molecule is formed upon the return of the H atom to the neighborhood of the trapped F atom from the ‘wrong’ side, i.e. with a krypton atom between them. The threshold temperature for the HRgF compound formation was found to be much lower for the stable SS site in a krypton matrix (7 K) than

for the DS site (31 K) and also for the DS site of argon (23 K). The very low threshold for the SS site formation indicates a mechanism by which the H atom is trapped in a compact site, in a metastable state. A slight motion suffices to 'release' it into the more stable configuration. The lower threshold for argon in the DS site is surprising, as the static barrier for HArF formation is higher than for HKrF. A possible explanation is that in a matrix the barrier height fluctuates due to the thermal motions of matrix atoms. In some configurations, the matrix atoms 'push' the atoms of the molecule towards the transition state making the barrier smaller. This effect is stronger for a tight environment, as in argon, than in a looser one, as in krypton.

In summary, the special case of these new compounds indicates the importance of less-stable matrix sites, such as interstitial ones. They are expected to be important in understanding the dynamics of small species, especially small atoms such as H and F.

### 4.3. *Planar molecules*

#### 4.3.1. *Naphthalene*

The $S_0$–$S_1$ electronic transition of naphthalene is forbidden, and its spectrum is expected to be sensitive to the local symmetry and environment. An MD simulation of naphthalene in an argon matrix [11] revealed three main trapping sites. In two of the sites, the molecule replaced four or five atoms in the {111} crystallographic plane, and in the third, four atoms in the {001} plane. The two {111} trapping sites were very similar as can be seen from the cuts shown in Fig. 5.

In the {111} 4S site only four argon atoms are replaced so that the molecule undergoes strong repulsive interactions with four argon atoms, marked by asterisks in the figure. These atoms are seen to be displaced away from their position in the neat argon crystal. In the {111} 5S site one of these atoms is removed, allowing for more space for the guest molecule. The displacement of the other three atoms from their natural locations is much smaller. The {001} site has a larger cavity and the argon atoms in the plane occupied by the guest molecule are not shifted from their normal lattice positions. However, since the distance between two {001} layers is much smaller than between two {111} layers (2.58 compared to 3.02 Å) several argon atoms in the neighboring {001} layers are strongly pushed outward from the guest, while no such shift is found in the {111} trapping sites.

In the experiment, two main trapping sites were observed (A and B): they were distinguished by the following main features:

(1) The origin of the $S_1 \leftrightarrow S_0$ transition was red-shifted with respect to the gas phase by 158 $cm^{-1}$ in site A and by 118 $cm^{-1}$ in site B.
(2) The relative intensity of $b_{1g}$-type vibronic bands in the $S_1 \rightarrow S_0$ fluorescence spectra compared to the origin or $a_{1g}$-type vibronic bands was smaller for site A than for site B.
(3) The fluorescence lifetime of site A was much shorter than for site B (24 vs 90 ns).
(4) The phosphorescence-to-fluorescence intensity ratio is larger in site A than in site B.
(5) The origin of the $T_1 \leftrightarrow S_0$ transition was red-shifted with respect to the gas phase by 173 $cm^{-1}$ in site A and only by 28 $cm^{-1}$ in site B.

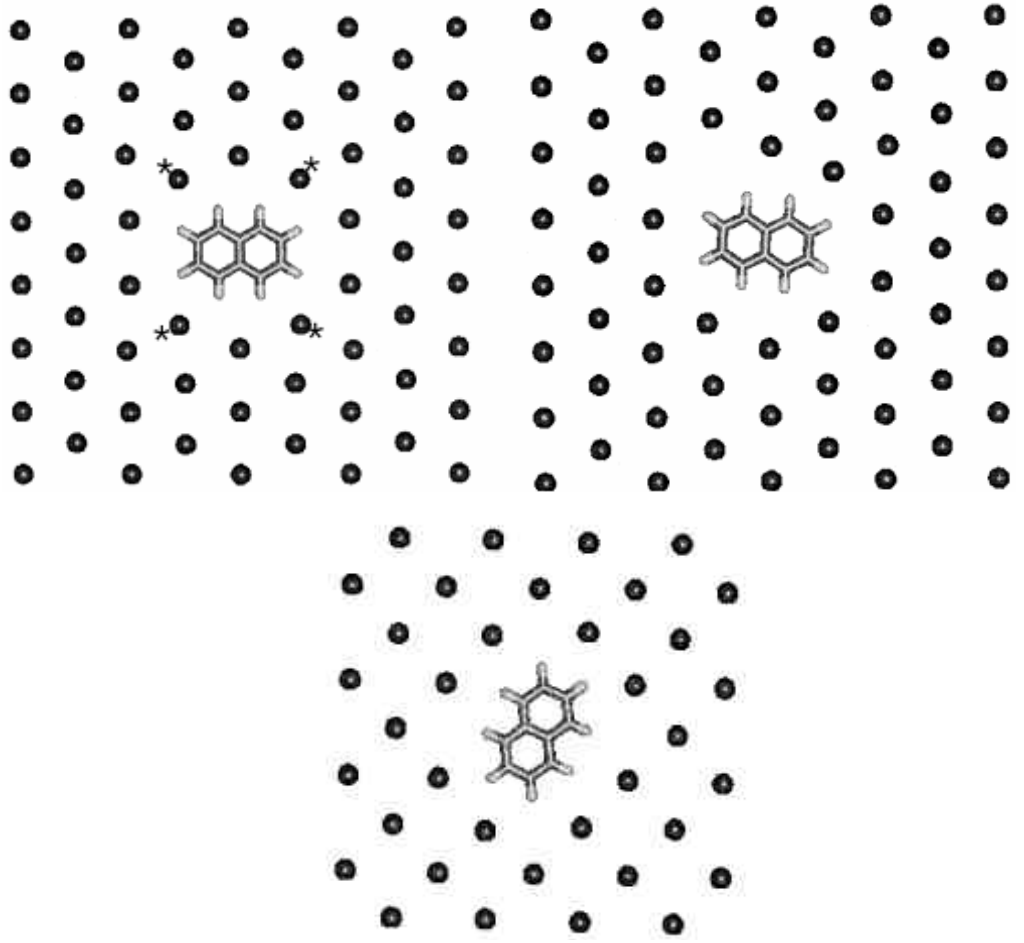

FIG. 5. Calculated trapping sites of naphthalene in solid argon. Top: the two {111} trapping sites, bottom the {001} trapping site (adapted from ref. 11).

(6) The phosphorescence bands are broader in site B than in site A, in which they are roughly as narrow as in fluorescence.

All these observations indicate a stronger interaction with the matrix of naphthalene in the $S_1$ state in site A. The authors suggest that site A should be identified with the {001} 4S site, and site B with the two {111} sites. The difference between the spectroscopic properties of the two {111} sites was considered to be too small to be detected experimentally. The following reasons are given for this assignment.

Intersystem crossing is more efficient in site A (points 3 and 4) due to the stronger interaction of naphthalene *p*-electrons with *p*-electrons of argon in neighboring crystallographic {001} layers. The stronger interaction of the *p* electrons of naphthalene with those of argon, which is mainly attractive, is the reason for the larger red-shift of the 0–0 bands of the $S_1 \leftrightarrow S_0$ and $T_1 \leftrightarrow S_0$ transitions (points 1 and 5).

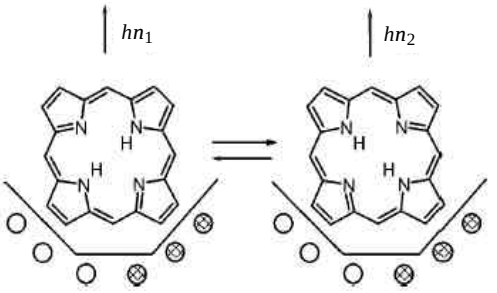


FIG. 6. Tautomerization in porphyrin, accompanied by a change in the relative position of the molecule with respect to the rigid environment (from ref. 40).

In the {111} trapping sites, the two neighboring crystallographic layers are further away from the trapped molecule than in the {001} site. Thus, some small amplitude motion is allowed in these sites, explaining the broadening of the bands in site B (point 6).

4.3.2. *Anthracene*

A complete description of the experiments and the analysis was given in previous publications [15, 35, 36]. Three main trapping sites were found in both the experiment and simulations; the reader is referred to these papers for details (see also Section 4.5).

4.3.3. *Porphyrin*

Porphyrin undergoes a photo-induced tautomerism reaction in which the two inner hydrogen atoms switch partners (Fig. 6).

In the gas phase, this reaction cannot be discerned in the spectrum due to the high symmetry of the molecule. However, as schematically shown in Fig. 6, in a matrix the microenvironment of the trapping site may be different. Indeed, line splittings have been observed in the electronic absorption and emission spectra of porphyrin, as well as in the IR spectra [37–39]. As shown in Fig. 7, the two components of the doublets appearing in the visible and IR spectra are of approximately equal intensity.

They have been assigned to two distinct trapping sites and narrow-band irradiation could be used to transform all molecules into one of the trapping sites. In order to establish the absolute assignment of the A and B bands, an MD simulation was performed. The MD method revealed that the main trapping site of porphyrin in solid xenon is a seven-atom substitutional site in a hexagonal cavity in the {111} crystallographic plane [40, 41]. The trapped porphyrin molecule can find itself in two different configurations in this trapping site, depending on the orientation of the two inner hydrogen atoms with respect to the surrounding cage (Fig. 8). In order to establish the absolute assignment, the matrix shifts were computed for the two possible orientations of the molecule in the site. In these trapping sites, the xenon atoms lying along the X-axis (marked by arrows) are the ones that interact most strongly with the trapped molecule. Along the Y-axis the neighboring atoms are not distorted from their native positions. The IR spectra were calculated based on the trapping sites' structures, including the two nearest coordination layers of xenon atoms. Calculations at DFT level for the IR spectra and TD-DFT for the electronic transitions revealed a small

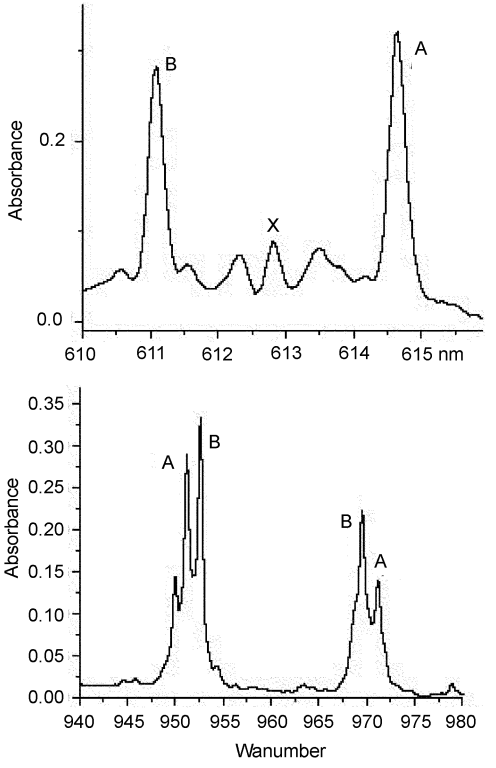


FIG. 7. Top, the electronic absorption in the 0–0 region of the $S_1$ transition; bottom, fragment of the IR spectrum of porphyrin in xenon at 5 K. The doublet components are labeled A and B. In the electronic spectrum, the location of site X (a minor additional trapping site) has also been indicated (from ref. 41)

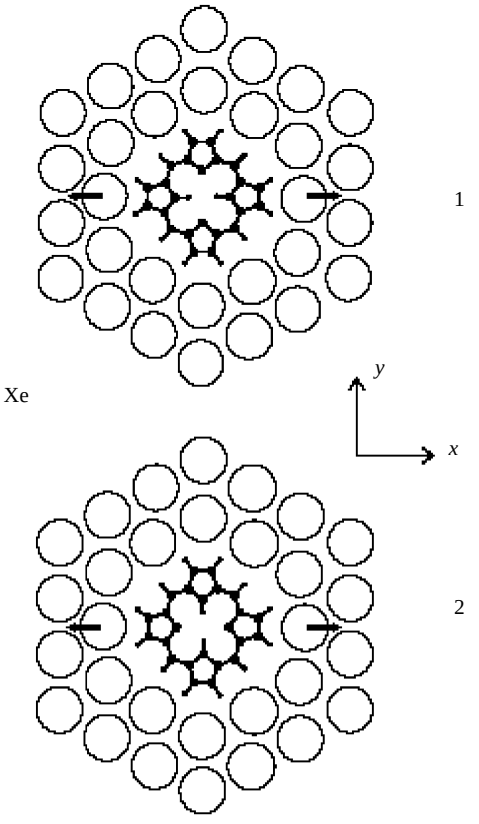


FIG. 8. A schematic representation of the structures of the two configurations of porphyrin in the {111} trapping site in a xenon matrix (from ref. 41).

shift for all IR bands. The direction of the shift (blue or red of structure 2 with respect to 1) varied according to the IR band, but was of the same sign as experimentally observed. In the majority of the cases, the sign of the calculated frequency shift agreed with the experimental one, allowing the absolute assignment of the geometry of the trapping site. Similar results and conclusions were obtained from the electronic spectrum.

### 4.4. *Nonplanar molecules*

For small molecules and also for large planar ones, the initial guess as to the form of the most stable trapping sites is intuitively simple, assuming that the matrix retains its overall crystalline order. Usually, the molecule is trapped along a single crystalline plane which needs to be selected. For nonplanar molecule, the initial guess is much less obvious, as a very large number of options open up. Two types of nonplanar systems were recently studied, both being benzene derivatives. Propylbenzene was chosen because it is the smallest aryl molecule having two stable conformations (*gauche* and *anti*) that can be easily dis-

cerned in the gas phase. Both are strongly fluorescent allowing sensitive detection at high dilution. Phenylpyrrole (PP) and pyrrolobenzonitrile (PBN) are two molecules exhibiting DF in a variety of solvents. The two emission bands are believed to arise from the fact that the molecules have at least two stable minima on the first singlet excited state surface. One is the 'normal' excited state (analogous to that of propylbenzene, which is due mainly to the excitation of the *p* electron system of the aromatic ring). It is referred to as the loclly excited (LE) state. The other is due to a charge transfer from the pyrrole moiety to the phenyl (or cyanophenyl) one and is termed the CT band. The CT band is strongly red-shifted in polar solvents, while the LE one shows the usual mirror image relation to the absorption spectrum. The resulting emission spectrum may contain contributions from both excited states, although in some solvents one of them may dominate. As the absorption spectrum of the molecules does not vary much upon changing the polarity of the solvent, initial excitation is believed to be due to the LE state and the CT one is formed by a nonradiative process which is thought to involve a large amplitude motion. The purpose of the study in argon matrixes was to find out whether the LE to CT transition can occur in the matrix, and thus help to elucidate the mechanism of this intramolecular charge transfer system. It turned out that the simulations underscored the importance of the cage effect and the limited translational and rotational motion in matrixes.

#### 4.4.1. *Matrix spectroscopy of propylbenzene* [42]

Propylbenzene was chosen for the study of trapping nonsymmetric molecules as the smallest benzene derivative that has two conformers (*gauche* and *anti*); this molecule was studied extensively in supersonic jets [43] and its low-temperature vibronic structure is therefore well known.

Three main band series assigned to different trapping sites of the *anti* and *gauche* conformers of the molecule were found in both absorption and emission spectroscopy. The relatively small number of trapping sites found for this asymmetric molecule appears surprising at first sight, but was found to be compatible with molecular dynamic simulations that nicely reproduced the small number of preferred sites.

Figure 9 demonstrates the advantage of fluorescence excitation compared to absorption spectra in the search for trapping sites. The main absorption bands are red-shifted with respect to the gas phase by about 110 $cm^{-1}$ and the different bands of a given conformer are separated by 20–40 $cm^{-1}$. The entire cluster distribution is spread over about 100 $cm^{-1}$. The emission spectra obtained upon selective excitation of the different trapping sites are displayed in Fig. 10. Comparison with the spectra of PP and PBN (which are also benzene derivatives, see below) clearly shows that an LE spectrum is vibrationally structured and allows easy discrimination between different trapping sites. Figure 10 clearly shows that in a matrix, a relatively large, asymmetric molecule can be electronically excited in a well-defined trapping site.

#### 4.4.2. *MD simulation of propylbenzene*

Sixty-five and sixty-eight runs were performed for the *anti* and *gauche* conformers in argon using the Fraenkel–Haas method. In order to reproduce the experimental distribution of

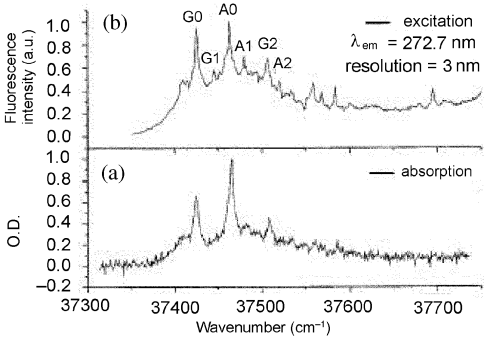


FIG. 9. The absorption and fluorescence excitation spectra of propylbenzene showing the origin region of the $S_0$–$S_1$ transition in an argon matrix. (a) Absorption spectrum at 0.1 Å spectral resolution, and (b) Laser-induced fluorescence excitation showing different sites. A and G stand for *anti* and *gauche* conformers of the molecule. Three sites are seen for each conformer (from ref. 42).

sites, the deposition temperature was 5 K and the fast cooling method [8] was applied. The molecules were treated as rigid bodies (the constraints were imposed by the RATTLE algorithm [44]). In order to minimize a possible bias due to the choice of the {001} as the exposed surface, the simulation was begun by randomly depositing 50 argon atoms prior to bringing in the guest molecule. The parameters used in the Lennard–Jones (LJ) potential are listed in Table I.

The resulting sites consisted of cavities in which 4–7 argon atoms were replaced. However, the trapping sites could be grouped into several classes in which larger sites were identical to smaller ones with one or two additional atoms replaced. In each class, the guest molecule was found to be positioned approximately as in the smallest cage or 'core'. Therefore, all sites with the same core are expected to exhibit very similar spectroscopic properties–the same assumption was made in the analysis of the experimental results obtained for naphthalene [11]. Using this classification, three trapping sites each were dominant (accounting for 80% of the runs) for both *anti* and *gauche* conformers. Table II lists the number of runs leading to each site and the site's relative energies. The corresponding trapping sites are shown in Fig. 11 in the cavity format (introduced in Scheweke *et al.* [52]). The

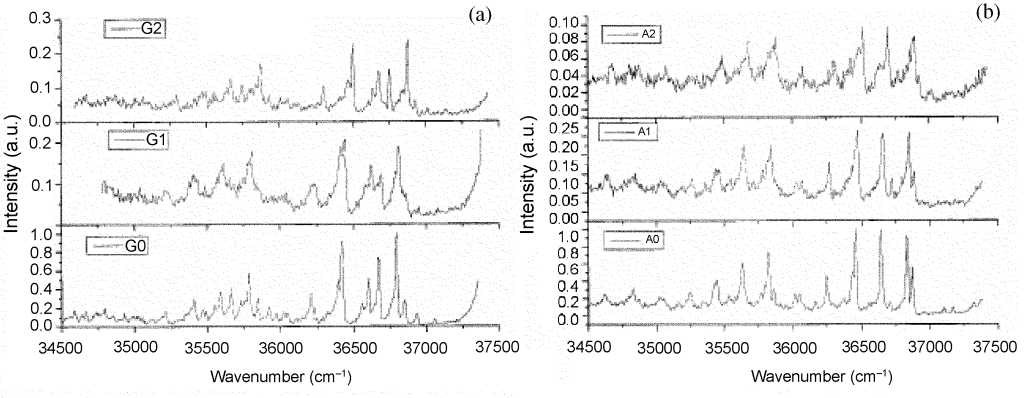


FIG. 10. Fluorescence spectra obtained upon excitation at some minor excitation peaks marked in Fig. 9. (a) Spectra obtained for the peaks marked $G_0$, $G_1$ and $G_2$ (from ref. 42). (b) Spectra obtained upon excitation at peaks marked $A_0$, $A_1$ and $A_2$.

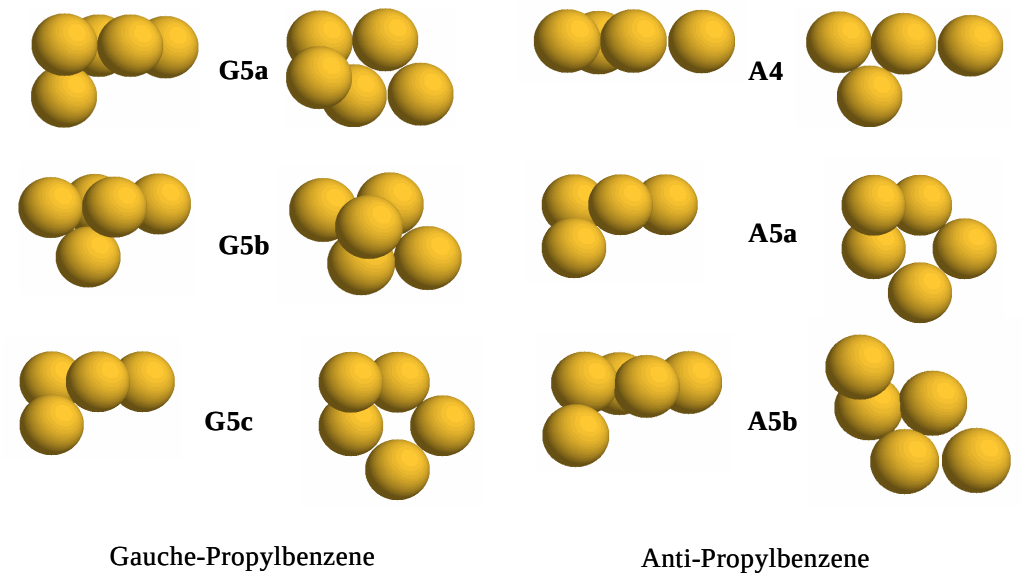


FIG. 11. The form of three frequently encountered cavities obtained from MD simulations of propylbenzene conformers (*gauche* and *anti*) in argon. The cavities are shown in two different projections: Top (right) and (side views (left). The cavity represents, in a space-filled model, the lattice atoms that have been replaced by the molecule. This illustration suggests the volume occupied by the molecule in each site and enables an easy comparison between different trapping site geometries.

forms shown represent the hollow space formed by the argon lattice atoms which have been removed by the host molecule. This representation allows an easy comparison between different trapping sites. For both conformers, one of the sites was obtained far more frequently

**Table I**
**Lennard–Jones (LJ) parameters used in the simulation of the trapping sites of phenylpyrrole (PP), pyrrolobenzonitrile (PBN) and propylbenzene in argon**

| Atom pair | $s$ (Å) | $e$(cm$^{-1}$) |
|---|---|---|
| Ar-Ar | 3.36 | 83.40 |
| Ar-C | 3.38 | 54.20 |
| Ar-N | 3.07 | 39.00 |
| Ar-H | 3.11 | 22.30 |

**Table II**
**Trapping sites obtained from the MD simulations of propylbenzene (*anti* and *gauche* conformers) in argon matrix.** The sites are shown in Fig. 11 in the cavity representation. $P$ is the probability of reaching a trapping site (assumed to equal the number of runs leading to the site divided by the total number of runs), $E_{site}$ is the corresponding site energy (see Appendix I for details of the calculation) and $\Delta E = (E_{site} - E_{fcc})/\langle E_{Ar}\rangle$, where $E_{fcc}$ is the energy of a perfect fcc lattice of the same size and $E_{Ar}$ is the average energy per argon atom in the perfect lattice (energies in kJ/mol).

| | Site | Ar atoms replaced | $P$ | $E_{site}$ | $\Delta E$ |
|---|---|---|---|---|---|
| *Gauche** | G5a | 5 | 35 | –5733.4 | 8.6 |
| | G5b | 5 | 26 | –5728.8 | 9.1 |
| | G5c | 5 | 18 | –5728.9 | 9.1 |
| *Anti** | A4 | 4 | 24 | –5738.7 | 7.9 |
| | A5a | 5 | 38 | –5731.4 | 8.8 |
| | A5b | 5 | 17 | –5726.4 | 9.4 |

*68 and 65 runs were made for the *gauche* and *anti* conformers, respectively. The energy of a pure argon matrix of same size is –5802.4 kJ.

than the others (site G5a for *gauche*-propylbenzene and site A5a for *anti*-propylbenzene). It should also be noted than only one of the cavities was found in common for the two conformers.

The trapping sites found for the *gauche* conformer consist of four argon atoms originating from a single lattice plane replaced by the benzene ring and an additional argon atom removed from an adjacent plane. In the two most frequently obtained sites (including the most stable one), the benzene ring lies in the {111} plane while in the third site, it lies in the {001} plane.

The *anti* conformer can be contained in smaller sites (in which only four argon atoms are substituted) than the *gauche* one. In the 4 substitutional site (4*S*), all the replaced atoms come from a {111} plane. The higher energy site is identical to the site termed G5b for the *gauche* conformer, in which the benzene ring lies in the {001} plane. In the third site of the *anti* conformer, the benzene ring replaces four argon atoms in the {111} plane and an additional one on top of them. The cavity thus formed differs from the corresponding *gauche* cavities (G5a and G5c) by the position of the substituted atom removed from the neighboring plane.

The trapping sites of propylbenzene were simulated also by Horinek and Dick [45] using the RSM (see Section 3) method. They found different sites but the most probable ones are in good agreement with those obtained by the Fraenkel–Haas (simulated deposition model-SDM) method. In fact, two and three sites were obtained very frequently for the *anti* and *gauche* conformers, respectively. The two main sites of *anti*-conformer correspond to sites A4 and A5a of SDM while the three sites of *gauche*-propylbenzene correspond to sites G5a, G5b (with an additional missing atom) and G5c of SDM.

The three main peaks observed experimentally for the 0–0 transition of the *anti* and *gauche* conformers in the fluorescence excitation spectrum are tentatively assigned to the three major trapping sites found for this conformer. The highest intensity peaks are attributed to the sites noted A5a and G5a, respectively, which were obtained with the highest probability.

#### 4.4.3. *PP and PBN*

These molecules, were studied in a matrix in order to clarify the mechanism of DF emitted in solution; their structures are shown in Fig. 12 along with the structure of dimethylaminobenzonitrile, the parent molecule. The experimental results in an argon matrix (neat and doped with AN) were recently published [46, 47] and will briefly be summarized here. The nonplanar form of these molecules (the pyrrole and phenyl rings are twisted from planarity in the ground state by 30–40°) makes it difficult to predict intuitively the form and size of their trapping sites. Moreover, experiments were also performed on argon matrixes doped with AN. The pyrrole derivative adduct with AN (whose calculated structures are shown in Fig. 13) is even more asymmetric than the bare molecule posing a still more challenging task in terms of the trapping site structure. Finally, there are several electronically excited states of these molecules, some of which are planar while in others the two rings are perpendicular to each other. The simulation of the trapping sites of all these species was car-

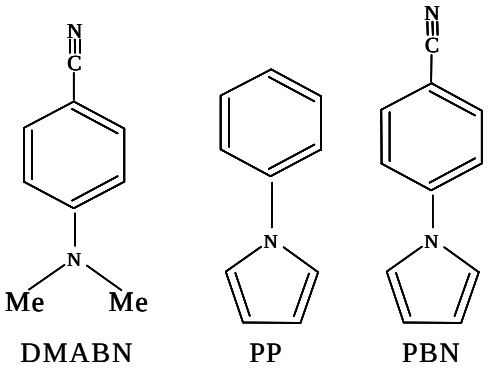


FIG. 12. The structure of some molecules exhibiting dual fluorescence.

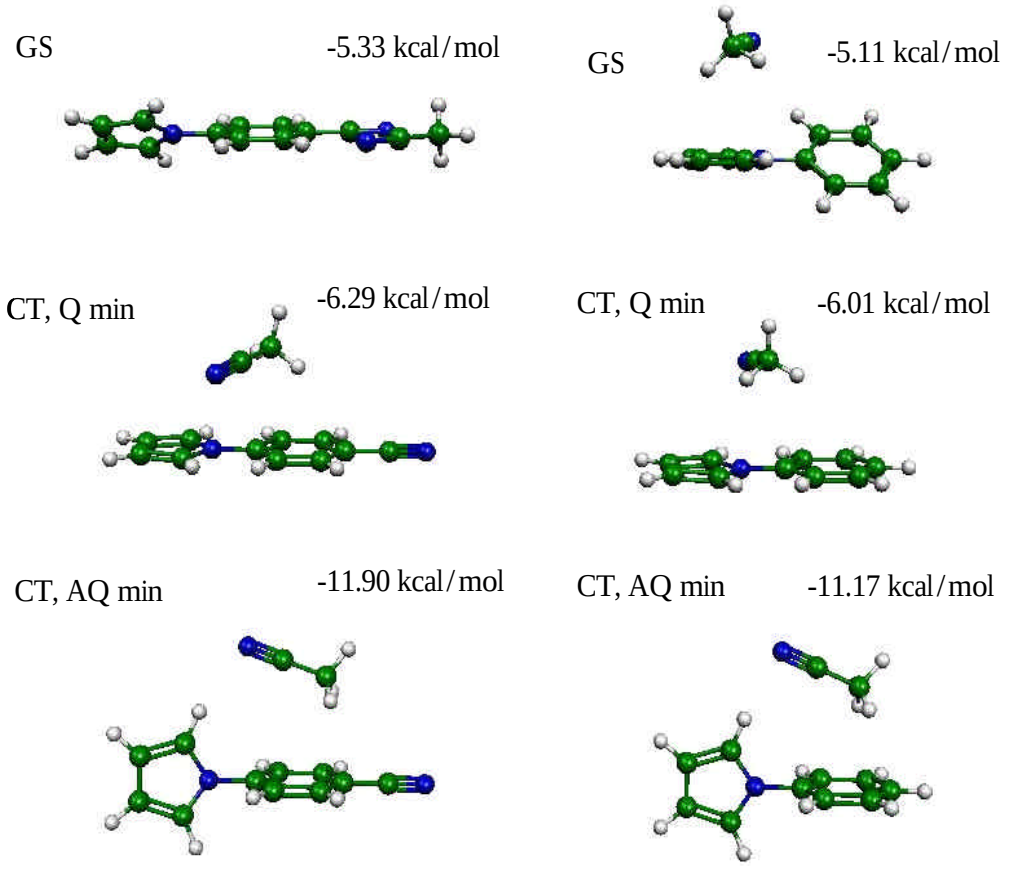


FIG. 13. The calculated equilibrium structures of the most stable PP : AN and PBN : AN adducts in the ground state and in the two CT excited states The energies signify stabilization with respect to the separated molecules (from ref. 47).

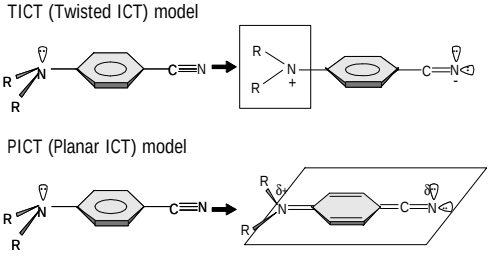


FIG. 14. A schematic presentation of the structure of the CT state according to the TICT and PICT models for PBN.

ried out for interpreting the photophysical behavior of these two molecules upon electronic excitation.

The relatively small solvent-dependence in the absorption spectrum contrasts with a very large dependence of the emission spectrum on the polarity of the solvent. These facts were taken as an indication that there are two low-lying excited states that can emit fluorescence: an LE and a CT state and since the optical transition from the ground state to the LE state is much stronger, light absorption is mainly into the LE band in all solvents. The appearance of a red-shifted emission upon using polar solvents is due to a nonradiative process transferring the system from the LE state to the CT one, which becomes the lowest excited singlet state in polar solvents. The fact that the CT state is not observed in absorption was explained by unfavorable Franck–Condon (FC) factors from the stabilized ground state structure. The FC argument was also evoked to account for the strong red shift in the emission spectrum of the 'anomalous' band.

Two main models have been considered to account for the formation of the CT state. Grabowski and coworkers [48] proposed a twisted model—the charge is transferred from the donor to the acceptor leading to two weakly coupled moieties bound by a single C–N bond. In the stable form of this state the amino group and the phenyl one are perpendicular to each other. This model is known as the twisted intramolecular charge transfer model (TICT). Zachariasse [49] and colleagues propose a different structure for the CT state – the charge transfer actually couples the two moieties more strongly, placing four electrons between the two in the form of a double bond. Consequently, the system becomes planar in the excited state. The acronym for this model is PICT (P for planar). A schematic representation of these models is given in Fig. 14.

Whereas the physical nature of the PICT model is clear, a CT structure can be obtained from the GS one by resonance—the rationale for the stability of the TICT state was not explained. In a 2002 paper [50], a quantum mechanical description for this state was offered, based on stabilization by allyl resonances in the phenyl ring. In the resultant structure, charge is separated between the two components (amino and phenyl groups). This form was termed antiquinoid (AQ) since the phenyl ring is stretched (the two central bonds elongate). This form turns out to be most stable when the phenyl and amino moieties are perpendicular to each other and therefore corresponds to the TICT model. Another CT structure was also found, in which charge alternates along the molecular frame, accounting for its smaller calculated dipole moment. This form is termed quinoid (Q) since the phenyl ring assumes a

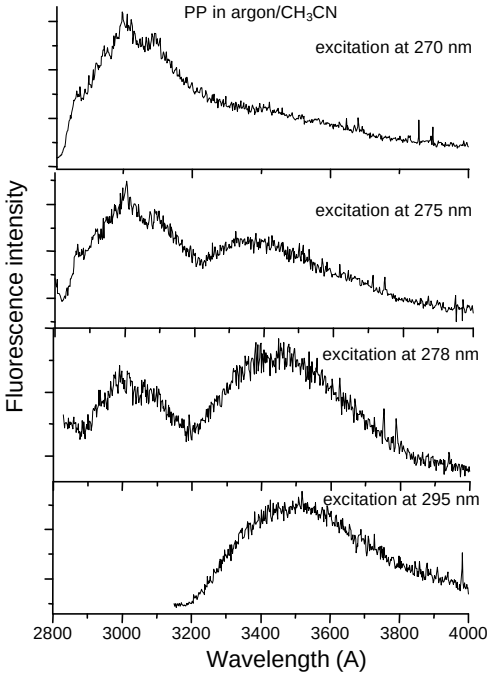


FIG. 15. Dual emission of PP in AN-doped argon matrixes as a function of excitation wavelength (from ref. 46).

quinoid structure (the two central bonds shorten), as does the CN bond. Since the two moieties are coplanar in this form, it corresponds to the PICT model. The minimum of the Q form was calculated to be lower in the gas phase than the AQ one. Thus, in strongly polar solvents the AQ form may be of lower energy than the Q one.

The main results of experiments in an argon matrix may be summarized as follows:

(1) PP was found to exhibit LE emission only in a neat argon matrix (14–30 K) while PBN exhibited both LE and CT bands.

(2) Addition of acetonitrile to the matrix led to a remarkable change in the PP spectrum: two bands were clearly discerned, similar to the solution phase. They were readily assigned to the LE and CT states (Fig. 15). In sharp contrast, addition of AN hardly affected the form of the PBN emission spectrum in an argon matrix, apart from the disappearance of the structured part of the spectrum, assigned to the LE state.

(3) The CT emission spectrum of PP in AN-doped argon matrixes was similar to the CT part of the emission spectrum of PP in AN solution (maxima at 350 and 357 nm, respectively). In contrast, the CT emission band in the spectrum of PBN in argon or AN-doped argon matrix appeared at significantly higher energy than in AN solution (330 nm compared to 480 nm).

MD simulations were carried out in an attempt to account for these results, in particular for the dramatic differences between the spectroscopic properties of PP and PBN in the matrixes. First, the trapping sites of both isolated molecules in an argon matrix were simulated [5]. The simulation method and the potential parameters used (Table I) were the same as for

**Table III**
**Trapping sites obtained from the MD simulations of PP and PBN in argon matrix. These sites are shown in Fig. 16 in the cavity representation. The parameters *P*, $E_{site}$ and $\Delta E$ are defined in Table II (energies in kJ/mol)**

| | Site | Ar atoms replaced | *P* | $E_{site}$ | $\Delta E$ |
|---|---|---|---|---|---|
| PBN* | 6a | 6 | 42 | –5740.7 | 7.7 |
| | 6b | 6 | 15 | –5733.7 | 8.5 |
| | 6c | 6 | 25 | –5733.4 | 8.6 |
| PP* | 5a | 5 | 15 | –5741.4 | 7.6 |
| | 6a | 6 | 21 | –5730.8 | 8.9 |
| | 6b | 6 | 19 | –5729.5 | 9.1 |

*52 and 53 runs were made for PBN and PP molecules, respectively.
Energy of a pure argon matrix of same size is -5802.4 kJ.

propylbenzene. The energies and probabilities of formation of the three most frequently encountered trapping sites are listed in Table III. The corresponding cavities are shown in Fig. 16. Then, the trapping sites in argon of the 1 : 1 clusters of PP and PBN with AN (both in the GS and in the excited CT states) were simulated [52]. In these simulations the clusters were treated as rigid bodies and deposited as such. Experimentally, the two constituents of the cluster are likely to arrive separately, and form the adduct upon being cooled by the matrix. A justification for the use of the cluster (which results in considerable saving of computer time) is that the 1 : 1 adduct's form represents the most stable configuration of the cluster. After one constituent is trapped on the surface, a cluster is formed only if argon atoms have not completely surrounded it prior to the arrival of the second ingredient. The latter causes local annealing, which allows for the attainment of the most stable form of the cluster, assuming that the interactions with neighboring argon atoms do not significantly change the pairwise interaction between the two polar molecules. The characteristic properties of the obtained trapping sites are given in Schweke *et al.* [52]. Briefly, the cavities of the GS-PBN:AN adduct have a structure different from that of the clusters of PBN in the CT state with AN, while the cavities of the GS-PP:AN adduct have a structure much closer to that of clusters of PP in the CT state with AN.

### 4.4.4. *Comparison with experiment*

Each trapping site suitable for the ground state molecule or cluster is fairly compact and impedes large amplitude motion of the trapped species. Franck–Condon excitation results in an excited state that finds itself in a structurally strained site, since the size, form and charge distributions of the molecule in the excited state are different than those of the ground state. Emission from a structurally relaxed CT state (as found in liquid solutions) can therefore be observed in an argon matrix only if the geometrical change required for stabilizing the CT state (primarily motion of the AN ligand with respect to the pyrrole derivative and rearrangement of the surrounding argon atoms) is small enough to be 'permit-

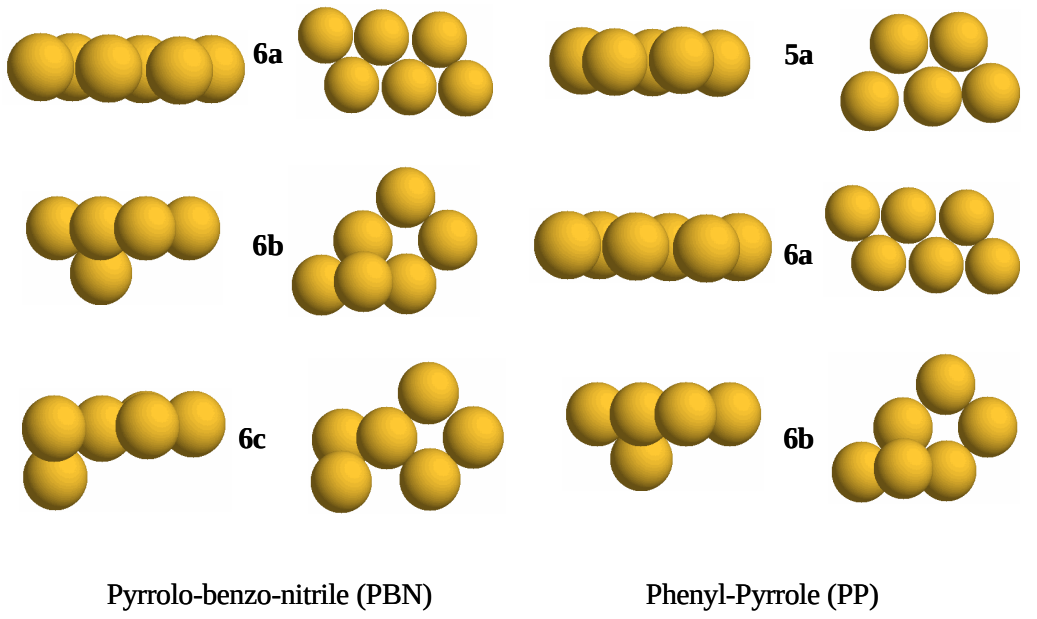


FIG. 16. The form of three frequently (for each molecule) encountered cavities obtained from the MD simulations of the PP and PBN molecules in argon (Details on the representation can be found in Fig. 11).

ted' by the matrix. A comparison between the trapping sites of the GS with those of the CT state clusters leads to the following conclusions:

*Neat argon matrixes*

Comparison of the GS trapping sites for PP and PBN with the CT ones shows that only a minor rearrangement is required to attain the preferred geometry of the Q-type site, while a more extensive one is needed to form the AQ-type one. Thus, it would appear that the CT emission of PBN in solid argon can be assigned to the Q (planar) form or to a strained AQ (perpendicular) form, which is not free to attain the ultimate minimum due to the cage effect. This explanation is consistent with the fact that the CT emission observed from PBN in argon (and AN/argon matrix) appears at significantly higher energy than in AN solution. The energy of the CT state of PP is too high in neat argon to be populated.

*AN-doped argon matrixes*

In the case of PBN, reorientation of the AN molecule to reach the optimal geometry of either of the CT minima is not likely in the matrix due to the large structural changes needed. Therefore, emission must ensue from the 'nascent' excited state structure and addition of AN to argon has nearly no effect on the recorded emission spectrum. This effect, called the Matrix Wall effect, is illustrated in Fig. 17. In the case of PP, reorientation of AN to stabilize the CT structure is restricted to a much lesser extent by the matrix. The addition of AN to argon thus leads to the apparition of CT emission.

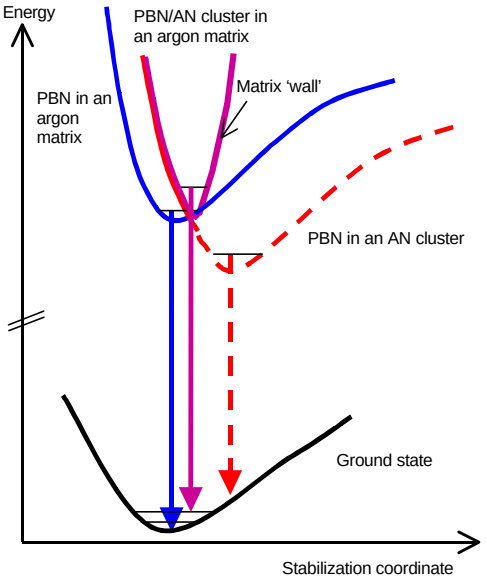


FIG. 17. A schematic presentation of the energy-level diagram of PBN in an argon matrix and in AN-doped argon matrix. The blue curve depicts the energy of the CT state in neat argon and the red one the expected curve in the presence of AN assuming complete structural optimization. The dashed curve shows the effect of the matrix: the barrier it creates leads to an effective potential that shifts the emission spectrum to the blue compared to the expected spectrum under full relaxation conditions.

The simulations of the pyrrole derivatives and their clusters were made under highly simplifying assumptions. Several improvements may be suggested: Only LJ potentials were assumed for the interaction of the guest with the matrix atoms, a term taking into account the polarizability of argon (eqn v(2) in Section 5) could be added. The LJ parameters for the excited states were the same as for the ground state. Only an fcc lattice was considered; it might be necessary to consider an hcp one also.

As far as the main goal of the simulations is concerned, it is likely that these modifications will not affect the qualitative conclusions. In all cases, a large number of argon atoms are replaced, and the main difference between the various trapping sites is their structure taken as a whole. Minor alterations due to somewhat different potentials are not expected to affect the conclusions. Furthermore, only a few trapping sites are experimentally resolved for both PP and PBN in neat argon, indicating that the differences between the various sites are not large. The widths of the observed lines for the $S_0 \rightarrow$ LE transition, ($\sim 100$ cm$^{-1}$), are much larger than those measured for propylbenzene. This finding probably indicates a large number of close-lying transitions due to different trapping sites as expected from the simulations. The addition of AN leads to an even broader spectrum, possibly due to a still larger number of nearly iso-energetic populated sites.

### 4.5. *Assessment of the MD method*

In this subsection, we discuss the determination of the relative energies of the systems obtained by the MD simulation, and its use for comparing the properties of different trapping sites. Once the final structure of a site is obtained, the energy of the whole system can be determined. The procedure applied is explained in detail in Appendix I. The energy determination provides a measure for the relative stability of different trapping sites of a given molecule; in particular, when several sites with the same number of substituted atoms are

obtained. In addition, the total site energy can be decomposed to the energy of the host crystal (with *n* atoms removed) and the energy of interaction between the guest molecule and the crystal [40]. The contribution of each lattice layer to this interaction energy can also be determined [11].

However, comparison of calculations made by different groups is usually difficult if not impossible, as at the moment there appears to be no standard procedure. The first and most obvious difficulty is that the energy of a matrix containing a trapping site must be determined on a finite cubic lattice 'cut' from the relatively infinite crystal. The size of the lattice portion is arbitrary and the energy depends on that choice. Therefore, comparisons are limited to the results obtained by the same method (which are mostly results obtained by the same group). Another difficulty in the determination of site energy arises when a given 'cage' (determined by the size and shape of the substituted atoms) leads to different trapping sites (determined by the orientation of the molecule in the cage), as mentioned in the introduction. Such trapping sites generally differ in spectroscopic properties and also slightly in energy. The example of porphyrin, whose two trapping sites show different spectral features both in the visible and in the IR absorption [38], was presented in Section 4.3. Another example is a cage of PP in argon in which either the pyrrole or the phenyl ring can be located in the {001} plane. The corresponding site energies differ by ~1 kJ/mol. A last issue relevant when calculating site energies is the distinction between the most stable and the most probable site. The major factor affecting the energy of a site is the number of lattice atoms substituted by the guest molecule: For a given guest, the most stable trapping site is the one in which the number of substituted atoms is minimal, even if the long-range distortion caused to the matrix is greater in this case [52]. Such a trapping site will rarely be formed experimentally while it may be obtained frequently from the simulation.

The simulated deposition conditions (for instance, the temperature of the template and the cooling rate) can influence the final distribution of sites. A simulation process allowing for local annealing leads preferentially the most stable site while 'fast-cooling' conditions [8] reproduce the experimental distribution (which is determined kinetically).

Several simulations of planar molecules in rare gas matrixes have been reported [11, 12, 40, 53], while very few studies on nonplanar big molecules (~20 atoms) are available at this time. Within the limited range of data, interesting conclusions can be drawn by comparing the site energies of molecules differing in the degree of symmetry (see Table II) [51]. The aromatic molecules, anthracene [15], PP [46], PBN [47] and propylbenzene [42] (*trans* and *gauche* isomers) have been studied experimentally in argon matrices and their trapping sites have been simulated.

In the two major sites of anthracence, the molecule replaces 6 argon atoms either in the {111} or in the {001} plane [15]. PBN also replaces mostly 6 argon atoms. In its most stable site, the 6 substituted atoms are removed from the same crystal plane (the {111} plane) while in the next two sites, of approximately the same energy, 5 atoms belong to the {001} plane and an additional atom belongs to the upper plane [52]. The fact that PBN lies in the {111} plane while it cannot substitute argon atoms from only one {001} plane is explained by the larger distance between adjacent {111} layers than between adjacent {001} layers. Although the {111} site is common to anthracence and PBN, the energy of this site

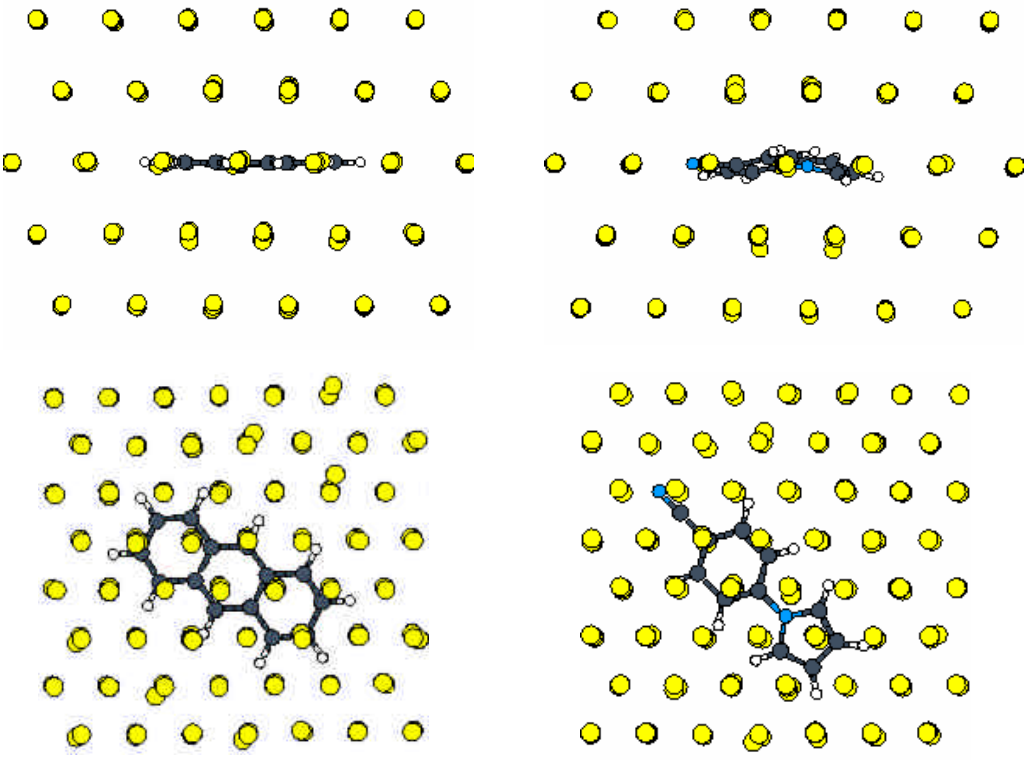

FIG. 18. A presentation of the six substitutional sites trapping of anthracene and PBN in the {111} lattice plane obtained by MD simulations. The dislocation of the neighboring argon atoms from their normal lattice positions is different for the two molecules.

is higher (by 7 kJ/mole) in the case of PBN than in the case of anthracene (Table III). The distortion to the structure of the lattice is comparable for both molecules (Fig. 18). Therefore, the different stability may be attributed to the fact that PBN needs to replace as much argon atoms from the lattice as anthracene, although it is a smaller molecule (21 compared to 24 atoms). This argument may also explain the fact that the {001} site of PBN is higher in energy than the {001} site of anthracene.

The trapping sites of PP resemble those of PBN and two of them (Table I) are common to both molecules. But for PP, a smaller site, in which the molecule replaces five atoms in the {111} plane, is obtained. The energy of this site is relatively high—very close to that of the corresponding 6 substitutional site (6SS) of PBN–since the PP molecule needs to shift significantly the surrounding argon atoms from their ideal lattice position in order to accommodate itself in this small site. The same behavior is observed when comparing the energies of the 5 SS of propylbenzene (*gauche* isomer) with the similar 6SS of PP. It appears from the comparison of the site energies presented in Table IV that the distortion caused to the lattice increases as the degree of symmetry of the guest molecule decreases. It may also be noticed that the number of different sites (even with the same number of substituted atoms) is higher for nonplanar molecules than for planar ones.

**Table IV**
**Energies of the main trapping sites obtained from MD simulations on molecules having different symmetries: Anthracene, PP, PBN and propylbenzene. The symmetry point groups are listed in Column 2. The site designation is the one used in the corresponding references and shown in Fig. 11 (for propylbenzene) and 16 (for PP and PBN). The characteristics of each site are indicated for clarity. The energies (in kJ/mol) were all calculated with the LJ parameters specified in Table I.**

| | Molecular symmetry group | Site | Main plane | Ar atoms replaced in main plane | $E_{site}$ | $\Delta E$ |
|---|---|---|---|---|---|---|
| Anthracene [15] | $D_{2h}$ | 6a | {001} | 6 | –5761.0 | 5.14 |
| (14 heavy atoms) | | 6b | {111} | 6 | –5756.2 | 5.73 |
| PBN [52] | | 6a | {111} | 6 | –5740.7 | 7.66 |
| (13 heavy atoms) | $C_2$ | 6b | {001} | 5 | –5733.7 | 8.53 |
| | | 6c | {001} | 5 | –5733.4 | 8.57 |
| PP [52] | | 5a | {111} | 5 | –5741.4 | 7.57 |
| (11 heavy atoms) | $C_2$ | 6a | {111} | 6 | –5730.8 | 8.89 |
| | | 6b | {001} | 5 | –5729.5 | 9.05 |
| Propyl-benzene (*Gauche*) | $C_1$ | G5a | {111} | 4 | –5733.4 | 8.57 |
| (9 heavy atoms) | | G5c | {001} | 4 | –5728.9 | 9.12 |

As mentioned above, anthracene, phenylpyrrole (PP), pyrrolobenzonitrile (PBN) and propylbenzene have been studied experimentally in argon matrices. In particular, their emission and excitation spectra have been recorded. When comparing the width of the vibronic bands, it appears that those of anthracence and propylbenzene are considerably narrower than those of PBN and PP (8 $cm^{-1}$ at 18°K for anthracene [35], 8.5 $cm^{-1}$ at 13°K and 12.5 $cm^{-1}$ at 250 K for propylbenzene [42] compared to more than 100 $cm^{-1}$ for PBN or PP at 25°K). Since there is no striking difference in the number or geometry of the cavities between the former and the latter molecules, the different width may be attributed to the torsional mode. In fact, this mode is not present in the planar anthracene molecule and it is rather high in energy in propylbenzene 43] (~ 350 $cm^{-1}$). In contrast, in PP or PBN, this vibrational quantum is rather low (66 $cm^{-1}$ in PP [54]) and can therefore be populated even at the low temperature of the matrix. Support for this explanation comes from the emission spectrum of biphenyl whose vibronic bands in argon matrix are broad [55] (~ 150–170 $cm^{-1}$).

## 5. Matrix sites and spectral shifts

A quantitative comparison of the simulation and experimental results requires the calculation of a property that varies with the trapping site structure and also a way to relate that property to experiment. The two most frequently used parameters that distinguish between trapping sites are spectral shifts (and line widths) on one hand, and reactivity on the other. Spectral shifts appear at first sight as the more straightforward approach: they can be measured very accurately, and in principle can be correlated with the site's structure. Nonetheless, it turns out that repeated efforts to calculate the spectral shifts were frustrated, as the fitting procedure is notoriously difficult. Part of the problem is that the matrix normally induces very small shifts (of the order of 0.1%) and that the calculation accuracy is not al-

ways that good. In this paper, we shall briefly consider only shifts of molecular vibrational levels which were more extensively studied than electronic transitions. The vibrational shifts of ground state molecules can be measured by infrared, Raman or dispersed fluorescence techniques. Experimentally, IR spectroscopy is more accessible so that the majority of available data comes from this technique.

Two main approaches were tried, which may be classified roughly as follows: (i) Classical solution of an oscillator in a field, treating the matrix as a perturbation, and (ii) Quantum calculations of a perturbed oscillator.

The usual approximation is to use a pairwise additive potential to represent the total potential energy of the matrix and guest molecule:

$$U_{M,\,g} = \sum_{i,\,j} V_{M,\,g}(r_i,\, R_j) \tag{1}$$

where $V_{M,g}$ stands for the interaction between the guest molecule $G$ and the matrix, $r_i$ are the coordinates of the $i$th atom of the guest molecule, and $R_j$ are the coordinates of the $j$th matrix atom. The summation runs over all pairs of atoms $(i, j)$.

The form of the pairwise potential varies, but it is convenient to partition it into electrostatic ($V^{el}$) and neutral ($V^{ne}$) interactions. Since the matrix atoms are not charged, the ($V^{el}$) term is dominated by charge-induced dipole interaction due to partial charges of the guest's atoms and the polarizability of the rare gas solid:

$$V^{el}_{M,\,g} = -a\,E^2(R_j)/2. \tag{2}$$

The neutral interaction term is approximated by a pairwise potential such as Lennard–Jones, Buckingham or others, whose parameters are deduced either from experiments or from a fitting to a high-level quantum mechanical calculation. For instance, the Lennard–Jones potential has the form:

$$V^{ne}_{M,\,g} = \sum_i V_i(|\,\mathrm{r}_u - \mathrm{R}_j\,|), \qquad V_i(\mathrm{r}) = 4e_i\left[\left(\frac{s_i}{r}\right)^{12} - \left(\frac{s_i}{r}\right)^{6}\right]. \tag{3}$$

The vibrational analysis is done as follows: Mass-weighted normal coordinates ($Q_1$, … $Q_k$ … $Q_N$) are used for the guest molecule's $N$ vibrational degrees of freedom. It is normally assumed that the total vibrational wave function can be written as the product of the separate $N$ wave functions of the normal coordinates

$$c(Q \cdots Q_N) = \prod_1^N c_k(Q_k). \tag{4}$$

The individual single-mode Schroedinger equations are solved separately for each oscillator:

$$\left(-\frac{1}{2}\frac{\partial^2}{\partial Q^2}+V_k(Q_k))\right)c_k(Q_k)=e_k\,c_k(Q_k). \tag{5}$$

The set of energies $e_k$ are the eigenvalues sought in this problem. The simplest approximation for the potential $V_k(Q_k)$ is the harmonic approximation, but it often fails to reproduce experimental results. In the vibrational self-consistent field (VSCF) method developed by Gerber and Jung [56], this potential is given by

$$V_i(Q_i)=\left\langle\prod_{k\neq j}^{N}c_k(Q_k)\,|V(Q_1,\cdots,Q_N\,|\prod_{k\neq j}^{N}c_k(Q_k)\right\rangle. \tag{6}$$

Equations (5) and (6) are solved iteratively.

The matrix shift in this approach is calculated in a straightforward way. The atoms of the molecule of the matrix are treated on the same footing: the normal modes of the system are in principle the normal modes of the whole ensemble. In practice, the molecular vibrational modes are of much higher frequency than those of the matrix, or of the matrix–molecule modes. Thus, the free molecule problem can be solved first, and the eigenvalues obtained can be entered as a first guess to the iterative procedure. In practice, various approximations are required to solve the problem. The number of matrix atoms that is actually used must be limited, in eqn (6); coupling between two normal modes only is allowed. Nonetheless, the method appears to be a very good starting point and has already been applied to some measured systems.

The question whether pairwise potentials can in principle reproduce the experimental matrix shifts has been addressed by several workers. Lakhlifi and coworkers showed computationally that indeed this can be done. Working on triatomic molecules ozone [24], $CO_2$ and $N_2O$ [25], they adopted the reverse procedure: knowing the experimental shifts, they varied the position of the trapped molecule in an assumed cage until a match with the experimental value was obtained. It was found that simple Lennard–Jones potentials were good enough for reproducing the matrix shifts correctly. The resulting site structures appeared reasonable, though the shifts of the argon atoms from their native lattice positions were somewhat larger than predicted by other simulations for similar molecules. It is not clear at this point whether the calculated structures are unique, or some other rearrangement of the crystal structure might also be suitable.

## 6. Summary and outlook (future prospects)

Considerable progress was made in the last 10–15 years towards the understanding of the microscopic structure of doped rare gas matrixes. In this paper, the present status of the MD method has been described. It is shown that the trapping sites of rather large and nonsymmetric structures can be predicted, and qualitatively compared with experiment. The example of PP and PBN along with their AN van der Waals adducts is described in some detail as it seems to be the most demanding system simulated so far.

The challenge for the near future is to develop a quantitative method for estimating the matrix shifts in the electronic and vibrational spectra of trapped molecules. Advances in computer technology indicate that the spectra of clusters (for instance, clusters of molecules with a small number of argon atoms) may soon be accessible by quantum chemical methods such as DFT, or perhaps even CI such as MRCI or CASSCF. The direct simulation of a matrix using quantum chemical methods is equivalent to the problem of predicting a crystal structure based only on the structure of the constituent atoms or molecules. This solid-state problem has not been solved yet so that the simulation of a matrix must for the time being start with a template that biases for the known structure of the crystal. A temporary solution to the problem may be sought by an MD simulation of the trapping of a cluster of the molecule with several argon atoms in a matrix.

The 'traditional' method for calculating solvent shifts was to use perturbation theory and consider separately the different contributing factors: electrostatic interaction due to permanent dipole moments, dipole-induced dipole interactions and dispersion forces (arising from second-order interactions) [57]. This method leads to approximate formulae that express the solvent shift as a function of the polarizabilities of the guest and host. Being a statistical theory it necessarily uses a mean-field approach which does not resolve small structural effects that can be measured in cryogenic matrixes.

A basic assumption of the MD method (as well as of the Monte-Carlo, one that is also often used) is that the experimental probability for obtaining a given site can be equated to the percentage of runs leading to it in the simulation. This assumption arises from the fact that the structure of a doped matrix is not determined by thermodynamic stability, but rather by kinetic factors (otherwise, only one trapping site is expected). Nonetheless, it is often found, as shown in many examples presented in this paper, that the most stable trapping site is also the most frequently encountered one in the simulation. The rationale is that statistically, in a dilute matrix (i.e. neglecting all guest–guest interactions), the guest should be distributed equally among all possible trapping sites. However, in the real trapping process, the final structure of a site is not determined by a single event, but by a long sequence of collisions, first of the guest with the host matrix, and later with other host molecules arriving from the gas phase. The local annealing caused by the interaction of the hot molecules with the cold surface appears to be the main mechanism by which the guest attains its final cage. A statistical theory of chemical dynamics is therefore justified. The final structure is determined by energy and entropic factors: the first is dominant as annealing can surmount small barriers and lead the system to the most stable local environment, provided the gross structure of the lattice is not perturbed. The entropic factor, which is often simply neglected, may be related to the number of possible lattice structures consistent with a given local minimum. This factor may be the cause for the (infrequent) cases in which the most stable structure is not the most frequently encountered one. A proper algorithm that will take this factor into account is also due.

**Acknowledgements**

We are deeply indebted to Dr R. Fraenkel who initiated the matrix isolation research in Jerusalem and to our colleagues Dr U. Samuni, Ms S. Kahana and Ms S. Dvir for the devoted

work and the important advances they made. We are grateful to Prof. B. Dick, Dr F. Molnar, Dr D. Horinek, Dr J. Pola and Dr R. Fajgar for their past and continued contributions to this project. Discussions with Prof. B. Gerber and Prof. A. Krylov were instrumental in launching the molecular dynamic simulation method. The generous support for the research in Jerusalem by The Israel Science Foundation founded by The Israel Academy of Sciences and Humanities and partially by The VolkswagenStiftung is gratefully acknowledged. The Farkas Center for Light Induced Processes is supported by the Minerva Gesellschaft mbH.

## References

1. Y. Haas, and U. Samuni, Reaction in rare gas matrices–matrix and site effects, *Prog. React. Kin.*, **23**, 211–279 (1998).
2. V. A. Apkarian, and N. Schwentner, Molecular photodynamics in rare gas solids, *Chem. Rev.*, **99**, 1481–1514 (1999).
3. M. Bargheer, and N. Schwentner, Particle transport phenomena in low-temperature solids, *Low Temp. Phys*., **29**, 165–175 (2003).
4. R. B. Gerber, Formation of novel rare-gas molecules in low-temperature matrices, *A. Rev. Phys. Chem*., **55**, 55–78 (2004).
5. E. Babka, E. Knozinger, and D. Hallamasek, Cage structure and long-range order in solid rare gas matrixes: A combined FTIR and XRD study, *J. Phys. Chem. A*., **105**, 8176–8182 (2001).
6. S. F. Ahmad, H. Keifte, and M. J. Clouter, On the solid–solid phase diagrams of Ar–$O_2$ and Ar–$N_2$ mixtures, *J. Chem. Phys*., **75**, 5848–5852 (1981).
7. C. Blindauer, M. Winter, O. Sild, G. Jansen, B. A. Hess, and U. Schurath, Rotational electronic splitting of matrix-isolated NH/ND A($^1\Delta$) in argon cages of $O_h$ and $D_{3h}$ symmetry–spectroscopic analysis and theoretical interpretation, *J. Phys. Chem*., **97**, 10002–10010 (1993).
8. R. Fraenkel, and Y. Haas, Molecular dynamics simulations of rare gas matrix deposition, *Chem. Phys*., **186**, 185–204 (1994).
9. X-J. Ning, and Q-Z. Qin, A new molecular dynamics method for simulating trapping site structures in cryogenic matrices, *J. Chem. Phys*., **110**, 4920–4928 (1999).
10. M. E. Riley, M. E. Coltrin, and D. J. Diestler, A velocity reset method of simulating thermal motion and damping in gas–solid collisions, *J. Chem. Phys*., **88**, 5934–5942 (1988).
11. C. Crépin, P. De Pujo, B. Bouvier, V. Brenner, and Ph. Millié, A simulation of naphtalene matrix isolation: Comparison with experiments, *Chem. Phys*., **272**, 243–258 (2001).
12. F. Molnár, and B. Dick, MD-simulation of site geometries and photoinduced site interconversion of diphenylacetylene (Tolan) in an argon matix, *Ber. Bunsenges. Phys. Chem*., **99**, 422–428 (1995).
13. D. Horinek, and B. Dick, Comparison of trapping sites of anthracene in hexagonal and cubic argon matrices: A molecular dynamics simulation study, *Zeit. Phys. Chem*., **214**, 811–822 (2000).
14. J. M. Haile, *Molecular dynamics simulations*, Wiley, p. 117 (1992).
15. R. Fraenkel, D. Schweke, Y. Haas, F. Molnar, D. Horinek, and B. Dick, Molecular dynamics simulations of site geometries of anthracene in an argon matrix, *J. Phys. Chem. A*, **104**, 3786–3791 (2000).
16. K. Vlaskonen, J. Eloranta, T. Kiljunen, and H. Kunttu, Thermal mobility of atomic hydrogen in solid argon and krypton matrices, *J. Chem. Phys*., **110**, 2122–2128 (1999).
17. T. Kiljunen, J. Eloranta, and H. Kunttu, *Ab initio* and molecular-dynamics studies on rare gas hydrides: Potential-energy curves, isotropic hyperfine properties, and matrix cage trapping of atomic hydrogen, *J. Chem. Phys*., **110**, 11814–11822 (1999).

18. L. Fredin, B. Nelander, and G. Ribbegard, On the dimerization of carbon dioxide in nitrogen and argon matrices, *J. Mol. Spectrosc*., **53**, 410–416 (1974).

19. A. Loewenschuss, and A. Givan, Raman and infrared spectra of matrix isolated $CO_2$ and $CS_2$, *Spectrosc. Lett*., **10**, 551–558 (1977).

20. R. Guasti, V Schettino, and N. Brigot, The structure of carbon dioxide dimers trapped in solid rare gas matrices, *Chem. Phys*., **34**, 391–398 (1978).

21. M. J. Irvine, J. G. Mathieson, and A. D. E. Pullin, The infrared matrix isolation spectra of carbon dioxide. II* Argon matrices: the $CO_2$ monomer bands, *Austr. J. Chem*., **35**, 1971–1977 (1982).

22. P. Brosset, R. Dahoo, B. Gauthier-Roy, L. Abouaf-Marguin, and A. Lakhkifi, Analysis of IR absorption spectrum of $O_3$ in inert matrices: spectroscopic evidence for two trapping sites, *Chem. Phys*., **172**, 315–324 (1993).

23. A. M. Vasserot, B. Gauthier-Roy, H. Chabbi, and L. Abouaf-Marguin, Spectroscopic studies of $(CO_2)$-C-13 trapped in rare gas matrices, *J. Mol. Spectrosc*., **220**, 201–208 (2003).

24. P. R. Dahoo, A. Lakhli, and H. Chabbi, Spectroscopy of $O_3$ trapped in rare gas matrices. I. Theoretical model for low-lying vibrational levels, *J. Chem. Phys*., **111**, 10192–10201 (1999).

25. A. Lakhli, H. Chabbi, P. R. Dahoo, and J. L. Teffo, A theoretical study of $CO_2$ and $N_2O$ molecules trapped in an argon matrix: Vibrational energies, and transition moments for low-lying levels and IR bar spectra, *Eur. Phys. J. D*, **12**, 435–448 (2000).

26. R. T. Hall, and G. C. Pimentel, Isomerization of nitrous acid: An infrared photochemical reaction, *J. Chem. Phys*., **38**, 1889–1897 (1964).

27. P. A. McDonald, and S. S. Shirk, The infrared laser photoisomerization of HONO in solid $N_2$ and Ar, *J. Chem. Phys*., **77**, 2355–2364 (1982).

28. P. M. Agrawal, D. L. Thompson, and L. M. Raff, Theoretical investigation of nonstatistical dynamics, energy transfer, and intramolecular vibrational relaxation in isomerization reactions of matrix-isolated HONO/Xe, *J. Chem. Phys*., **101**, 9937–9945 (1994); Theoretical studies of the effects of matrix composition, lattice temperature, and isotopic substitution on isomerization reactions of matrix-isolated HONO/Ar, **102**, 7000–7005 (1995).

29. L. Khriachtchev, J. Lundell, E. Isoniemi, and M. Räsänen, HONO in solid Kr: Site-selective *trans*↔*cis* isomerization with narrow-band infrared radiation, *J. Chem. Phys*., **113**, 4265–4273 (2000).

30. T. Talik, K. G. Tokhadze, and Z. Mielke, Infrared spectra and molecular dynamics simulations of *trans*-HONO isomer in an argon matrix, *Phys. Chem. Chem. Phys*., **2**, 3957–3966 (2000).

31. T. Talik, K. Tokhadze, and Z. Mielke, Infrared spectra and molecular dynamics simulations of *cis*-HONO isomer in an argon matrix, *J. Mol. Struct*., **611**, 95–102 (2002).

32. L. Khriachtchev, M. Pettersson, N. Runeberg, J. Lundell, and M. Räsänen, A stable argon compound, *Nature* (*Lond.*), **406**, 874–876 (2000).

33. M. Pettersson, L. Khriachtchev, A. Lignell, M. M. Räsänen, Z. Bihary, and R. B. Gerber, HKrF in solid krypton, *J. Chem. Phys*., **116**, 2508–2515 (2002).

34. Z. Bihary, G. M. Chaban, and R. B. Gerber, Vibrational spectroscopy and matrix-site geometries of HArF, HKrF, HXeCl, and HXeI in rare-gas solids, *J. Chem. Phys*., **116**, 5521–5529 (2002).

35. R. Fraenkel, U. Samuni, Y. Haas, and B. Dick, A matrix isolation study of the fluorescence of anthracene and anthracene–ammonia adducts in solid argon, *Chem. Phys. Lett*., **203**, 523–530 (1993).

36. J. Wolf, and G. Hohlneicher, High-resolution one- and two-photon spectra of matrix-isolated anthracene, *Chem. Phys*., **181**, 185–208 (1994).

37. J. Radziszewski, J. Waluk, and J. Michl, FT visible absorption-spectroscopy of porphine in noble-gas matrices, *J. Mol. Spectrosc*., **140**, 373–389 (1990).

38. J. Radziszewski, J. Waluk, and J. Michl, Site-population conserving and site-population altering photoorientation of matrix-isolated free-base porphine by double proton transfer: IR dichroism and vibrational symmetry assignments, *Chem. Phys*., **136**, 165–180 (1989).

39. J. Radziszewski, J. Waluk, M. Nepras, and J. Michl, Fourier-transform fluorescence and phosphorescence of porphine in rare-gas matrices, *J. Phys. Chem.*, **95**, 1963–1969 (1991).

40. A. Krychenko, and J. Waluk, Molecular dynamics simulations of matrix deposition. I. Site structure analysis for porphyrin in argon and xenon, *J. Chem. Phys*., **119**, 7318–7327 (2003).

41. A. Krychenko, A. Gorski, and J. Waluk, Molecular dynamics and density functional theory simulations of matrix deposition. II. Absolute site structure assignment for porphyrin in xenon, *J. Chem. Phys*., **121**, 12017–12025 (2004).

42. S. Dvir, and Y. Haas, Matrix isolation spectroscopy of propylbenzene conformers and trapping sites, *J. Chem. Phys*., **114**, 7361–7367 (2001).

43. (a) J. B. Hopkins, D. E. Powers, and R. E. Smalley, Vibrational relaxation in jet-cooled alkyl benzenes. I. Absorption spectra, *J. Chem. Phys*., **72**, 5039–5048 (1980); (b) J. B. Hopkins, D. E. Powers, S. Mukamel and R. E. Smalley, Vibrational relaxation in jet-cooled alkyl benzenes. II. Fluorescence spectra, *J. Chem. Phys*. **72**, 5049–5061 (1980).

44. H. C. Andersen, Rattle: A 'velocity' version of the shake algorithm for molecular dynamics calculations, *J. Comp. Phys*., **52**, 24–34 (1983).

45. D. Horinek, *Theoretical investigations of spectroscopy and photochemistry of matrix isolated molecules*, Ph.D. Dissertation, University of Regensburg (2000).

46. D. Schweke, and Y. Haas, The fluorescence of N-phenylpyrrole in an argon/acetonitrile matrix, *J. Phys. Chem. A*, **107**, 9554–9560 (2003).

47. D. Schweke, H. Baumgarten, Y. Haas, W. Rettig, and B. Dick, Charge-transfer-type fluorescence of 4-(1H-pyrrol-1-yl)benzonitrile (PBN) and N-phenylpyrrole (PP) in cryogenic matrices: Evidence for direct excitation of the CT band, *J. Phys. Chem. A*, **109**, 576–585 (2005).

48. K. Rotkiewicz, K. H. Grellman, and Z. R., Grabowski, Reinterpretation of the anomalous fluorescence of *p*-N,N-dimethylaminobenzonitrile, *Chem. Phys. Lett*., **19**, 315–318 (1973).

49. K. A. Zachariasse, M. Grobys, Th. von der Haar, A. Hebecker, Yu. V. Il'chev, Y.-B. Jiang, O. Morawski, and W. Kühnle, Intramolecular charge transfer in the excited state. Kinetics and configurational changes, *J. Photochem. Photobiol. A: Chem*., **102**, 59–70 (1996).

50. S. Zilberg, and Y. Haas, The nature of the intramolecular charge transfer excited state in *p*-pyrrolo-cyanobenzene (PBN) and other derivatives of benzene substituted by electron donor and acceptor groups, *J. Phys. Chem. A*, **104**, 1–11 (2002).

51. The procedure used to calculate the site's energies is described in the Appendix. As different groups use different Lennard–Jones parameters, the numerical energy values reported here may differ from those found in the literature. However, site structures turn out to be little affected by these small differences in the values of the parameters.

52. D. Schweke, Y. Haas, and B. Dick, Photophysics of phenylpyrrole derivatives and their acetonitrile clusters in the gas phase and in argon matrices: Simulations of structure and reactivity, *J. Phys. Chem. A*, **109**, 3830–3842 (2005).

53. I. Biktchantaev, V. Samartsev, and J. Sepiol, Perylene and terrylene in rare gas matrixes: spectroscopic and computational studies of inclusion sites, *J. Luminesc*., **98**, 265–272 (2002).

54. K. Okuyama, Y. Numata, S. Odawara, and I. Suzuka, Electronic spectra of jet-cooled 1-phenylpyrrole: Large-amplitude torsional motion and twisted intramolecular charge transfer phenomenon, *J. Chem. Phys*., **109**, 7185–7196 (1998).

55. A. Baca, R. Rosseti, and L. E. Brus, Structure and dynamics of the biphenyl ring torsion in solid neon and argon, *J. Chem. Phys*., **70**, 5575– 5581 (1979).

56. R. B. Gerber, and J. O. Jung, *Computational molecular spectroscopy* (P. R. Bunker, and P. Jensen, eds), Wiley (2000).

57. See for instance, Y. Ooshika, *J. Phys. Soc. Jap.*, **9**, 594 (1954); H. C. Longuet-Higgins and J. A. Pople, Electronic spectral shifts of nonpolar molecules in nonpolar solvents, *J. Chem. Phys*., **27**, 192–194 (1957).

58. M. L. Klein, and J. A. Venables, *Rare gas solids*, Academic Press (1976).

## Appendix I

### Description of the SDM method and the relative energies of trapping sites

SDM is based on mimicking the experimental deposition process. A finite rectangular template (a typical size is 6*6*2 ($x$*$y$*$z$) cell units) is constructed using the experimental temperature-dependent argon lattice parameters [3]. The template is held at a desired temperature, which is kept constant during the whole deposition process by periodically scaling the velocities of all atoms. In the simulation, argon atoms (or guest molecules) coming from the z-direction are allowed to impinge on the x*y surface of the template, which is allowed to grow *only* in the z-direction. It is convenient to use the {001} plane as the exposed surface due to the use of periodic boundary conditions (see below) although experimental evidence shows that the {111} plane is normally the fastest growing one during a gas-phase deposition of argon [58]. In order to minimize a possible bias due to the choice of the {001} as the exposed surface, the simulation is begun by randomly depositing 50 argon atoms on the template. The exposed surface is thus significantly modified. Then, the guest molecule (treated as a rigid body, using the RATTLE algorithm [6]) is added to the system followed by additional argon atoms. The Velocity Verlet integrator [6] is used to solve Newton's equations of motion with a time step ($\Delta t$) short enough to justify linear dependence on $\Delta t$ (typical values are 1–3 fs). The interactions between atoms are approximated as the sum of pairwise contributions. An often used form is a Lennard–Jones (LJ) potential:

$$V_{\text{int}} = \sum_{a \in A} \sum_{b \in B} 4\varepsilon_{ab} \left[ \left( \frac{\sigma_{ab}}{R_{ab}} \right)^{12} - \left( \frac{\sigma_{ab}}{R_{ab}} \right)^{6} \right].$$

In this equation, $\varepsilon$ is the well depth of the interaction between atoms $i$ and $j$, $\sigma$, the contact distance, and $R$, the distance between the two atoms. The parameters $\sigma$ and $\varepsilon$ are usually obtained from fitting of experimental data in the bulk or in molecular beam experiments.

Periodic boundary conditions are imposed on the x and y directions, in order to compensate for the finite size. A cutoff parameter, defined as the interatomic separation at which the interaction is arbitrarily set to zero, is taken to be large enough to ensure that interactions between atoms separated by larger distances are negligible, but smaller than the template's linear x- or y-dimension. A typical value is $2.7\sigma$ for the relevant pairs. The added species (host or guest) bear initial velocities selected from a 300 K distribution and are placed in a random position that is separated from the template by a distance slightly smaller than the cutoff parameter. The added species is accelerated towards the surface under the attractive potential, hits it, and eventually is cooled to the template's temperature. The fast-cooling method [3] is applied to minimize the effect of local annealing around the point of impact caused by the warming of the template's atoms. The system is allowed to equilibrate for a period much longer than $\Delta t$ before a second species is added. Realistic mimicking of experimental conditions would require an impractical long delay period. In practice, 3–40 ps intervals between consecutive additions are commonly used, and the deposition process continues until the total number of atoms is at least double the initial one. Throughout the deposition, all interactions are allowed (apart from intramolecular ones–the deposited molecule is usually considered to be a rigid body), and all atoms are allowed to move.

### The stability of trapping sites

A finite chunk of the lattice is chosen for the energy calculations; in the examples used in the text it is 6*6*5 unit cells. Since the crystal grows by adding argon atoms to the template, the growth is not uniform and atoms are often accidentally missing from the lattice layers formed by the deposition. The first step in calculating the energy of a given trapping site is thus to ensure that the only missing atoms are those replaced by the guest molecule. This is done by adding argon atoms at the fortuitously empty lattice positions. Next, the system is warmed to 35 K in order to allow all the argon atoms to gain their optimum lattice positions. At this relatively high temperature, the system is equilibrated for about 50 ps, mimicking annealing and then gently cooled to 0.01 K. After waiting at the lower temperature for equilibration (15 ps are typically allowed), the total energy of the system is calculated. This energy is set equal to the total energy of interaction between the molecule and the lattice atoms and between each pair of lattice atoms. At the final low temperature, the kinetic energy of the system is negligible compared to the potential energy, which in turn is largely due to the attractive part of the potential. The energy is calculated with respect to a standard where the guest and all host atoms are infinitely separated from each other. During the annealing process, periodic boundary conditions are applied along all directions. The distortion of the matrix by the guest molecule is evaluated by comparing the position of the solvent atoms around the guest molecule with their positions in a perfect fcc lattice.

### Abbreviations

AN: acetonitrile
AQ: antiquinoid
CASSCF: complete active space self-consistent field
CI: configuration interaction
CT: charge transfer
DF: dual fluorescence
DFT: density functional theory
DS: double substitutional
ESR: electron spin resonance
fcc: face centered cubic
F–H: Fraenkel–Haas
hcp: hexagonal close-packed
IR: infrared
LE: locally excited
MD: molecular dynamics
MRCI: multi-reference CI
QC: quantum chemical
PBN: pyrrolobenzonitrile
PP: N-phenylpyrrol
RG: rare gas
RSM: random search model
SDM: simulated deposition model
SS: single substitutional
TD-DFT: time-dependent DFT
UV-VIS: ultraviolet-visible
VSCF: vibrational self-consistent field